White Rose Research Online

eprints@whiterose.ac.uk
https://eprints.whiterose.ac.uk
Universities of Leeds, Sheffield and York

Deposited via The University of Sheffield.

White Rose Research Online URL for this paper:
https://eprints.whiterose.ac.uk/id/eprint/247198/

Version: Published Version

Article:
Macartney, R.A., Budharaju, H., Smith, A.M. et al. (2026) Electrospun intraoral patches for the directional delivery of therapeutics; a potential treatment for oral lichen planus. Materials Today Advances, 32. 101023. ISSN: 2590-0498

https://doi.org/10.1016/j.mtadv.2026.101023

Reuse
This article is distributed under the terms of the Creative Commons Attribution (CC BY) licence. This licence allows you to distribute, remix, tweak, and build upon the work, even commercially, as long as you credit the authors for the original work. More information and the full terms of the licence here:
https://creativecommons.org/licenses/

Takedown
If you consider content in White Rose Research Online to be in breach of UK law, please notify us by emailing eprints@whiterose.ac.uk including the URL of the record and the reason for the withdrawal request.

UNIVERSITY OF LEEDS
University of Sheffield
UNIVERSITY of York

Materials Today Advances 32 (2026) 101023

Contents lists available at ScienceDirect

Materials Today Advances

journal homepage: www.journals.elsevier.com/materials-today-advances/

Electrospun intraoral patches for the directional delivery of therapeutics; a potential treatment for oral lichen planus

Robyn A. Macartney [a], Harshavardhan Budharaju [b,c], Andrew M. Smith [d], Shosei Kishida [e], Stefano Fedele [f,g], Ipsita Roy [b,c,h], Jonathan C. Knowles [a,*]

[a] Division of Biomaterials and Tissue Engineering, University College London (UCL), Eastman Dental Institute, London, United Kingdom
[b] School of Chemical, Materials & Biological Engineering, Faculty of Engineering, University of Sheffield, Sheffield, United Kingdom
[c] Insigneo Institute of Health Technology, University of Sheffield, United Kingdom
[d] Department of Microbial Diseases, UCL Eastman Dental Institute, Royal Free Campus, University College London, London, United Kingdom
[e] Department of Biochemistry and Genetics, Kagoshima University Graduate School of Medical and Dental Sciences, 8-35-1 Sakuragaoka, Kagoshima, 890-8544, Japan
[f] UCL Eastman Dental Institute, University College London, London, United Kingdom
[g] NIHR UCLH Biomedical Research Centre, London, United Kingdom
[h] PHAsT Ltd, The Innovation Centre, 217 Portobello, Sheffield, United Kingdom

ARTICLE INFO

Keywords:
Electrospinning
Polyhydroxyalkanoates
Wound healing
Oral lichen planus
Chronic inflammation
Oral disease

ABSTRACT

Oral mucosal diseases are difficult to treat due to the poor retention of the dosage form at the lesion site because of salivary washout. Additionally, the interactions of commonly applied corticosteroids with off-target tissues over long term treatment periods commonly lead to the development of secondary fungal infections. To address this a gradient electrospinning technique has been developed to enable the directional delivery of clobetasol propionate ensuring the targeted delivery of corticosteroid to the lesion site and minimal drug interaction with the rest of the oral cavity. As a preventative to the development of fungal infection and treatment of any pre-existing fungal infection, fluconazole is also loaded throughout the patch for universal delivery throughout the oral cavity. The developed patches showed good spatial separation of the drug loading and appropriate mechanical properties for use in oromucosal applications. The formulations were cytocompatible with oral epithelial cells and successfully restored healing in an *in vitro* inflammatory challenged scratch assay model. The results show that the patches developed demonstrate potential as a therapeutic platform in the treatment of oral inflammatory diseases such as lichen planus.

1. Introduction

Oromucosal drug delivery routes have been rising in popularity throughout recent years [1]. Several transmucosal delivery systems have been described such as bioadhesive tablets, gels, patches and films. These systems are particularly useful in scenarios which; require bypass of the first-pass metabolism, involve patients with dysphagia, require treatment of local oral cavity disease or management of chronic conditions. Given the unique anatomical and physiological conditions of the oral cavity they offer an extremely efficient route for systemic absorption of drugs [2]. The highly vascularised nature of these tissues enables rapid absorption and onset of action in comparison to conventional tablets [3]. In comparison to dermal tissues the oral mucosa generally offers higher permeability allowing for improved passive diffusion of many drugs as described by Bácskay where the skin showed a permeability constant of 44×10^{-7} cm/min compared to values of 470 – 973×10^{-7} cm/min for various areas of the oral mucosa [2]. Delivery via the mucosal tissues leads to direct entry into the systemic circulatory system avoiding potential degradation by digestive enzymes in the gastrointestinal tract and metabolism in the liver. Avoidance of the digestive tract also allows for the harsh gastric pH environment to be bypassed improving bioavailability, particularly for peptide or protein-based medications which are easily degraded by such conditions [4]. Finally, in comparison to intravenous or intramuscular injection, oromucosal systems are non-invasive easy to administer and provide a more convenient solution for patients which may lead to better compliance with treatment regimens.

The development of mucoadhesive drug delivery systems for the

* Corresponding author.
E-mail address: j.knowles@ucl.ac.uk (J.C. Knowles).

https://doi.org/10.1016/j.mtadv.2026.101023
Received 3 July 2026; Received in revised form 12 October 2026; Accepted 13 October 2026
Available online 17 October 2026
2590-0498/© 2026 The Authors. Published by Elsevier Ltd. This is an open access article under the CC BY license (http://creativecommons.org/licenses/by/4.0/).

treatment of oral mucosal diseases such as oral lichen planus (OLP), recurrent aphthous stomatitis (RAS), oral candidiasis or oral mucositis may revolutionise treatment regimens in this field [5]. Utilising mucoadhesive patches, films or gels offers the opportunity to provide prolonged, targeted and effective treatment to minimise pain and limitations surrounding rapid salivary clearance. Whilst such interventions may be useful for the treatment of multiple oral mucosal diseases, in this study we will focus on the treatment of OLP as it is a particularly troublesome condition for patients.This chronic inflammatory condition is caused by abnormal immune responses causing T lymphocytes to interfere with the oral mucosal membrane cells. This disease typically affects over 40's and there is no known cure, with most treatments focusing on symptom management. There are several symptoms which lead to diagnosis of OLP, the most common form being reticular which presents in white lacy patches on the buccal surfaces and the tongue [6]. The more disruptive form is erosive and appears as red, swollen tissues and open sores which cause severe burning, pain and sensitivity during eating, speaking and talking [7]. The aetiology of the disease is not fully understood but some triggers are widely recognised such as; immune system dysfunction, stress, trauma and administration of certain medications. The current treatment regimens include long-term management using topical corticosteroids in the form of oral gels, creams and mouthwashes [8]. However, the therapeutic potential of these formulations is limited by their short retention time at the lesion site, resulting in reduced drug exposure, limited efficacy and high recurrence rates [9]. Salivary washout can rapidly remove the therapeutic agent from the target site and increase drug interaction with off-target tissues which over long-term treatment regimens can lead to secondary complications such as oral candidiasis and mucosal atrophy [10]. Finally, in a small number of cases, approximately 0.5-2.5%, risks of malignant transformation to oral squamous cell carcinoma are reported [11]. In contrast the development of a mucoadhesive patch could provide prolonged retention at the lesion site and enable localised, controlled delivery or therapeutics, thereby increasing drug exposure at the target tissue whilst potentially reducing salivary washout and off-target exposure. This approach could therefore improve the efficacy and consistency of local drug delivery while reducing some of the limitations associated with repeated administration of conventional topical formulations, such as a lack of patient compliance to the treatment regimen.

Novel transmucosal drug delivery systems are non-invasive technologies which are designed to deliver therapeutics systemically through the mucosal membranes. Within the oral cavity these may be via a buccal, sublingual or gingival route. Depending on specific designs these may rely on passive diffusion, active or stimuli responsive delivery. Often these systems are fabricated using polymers such as carboxymethyl cellulose, polyvinylpyrrolidone, chitosan, polyethylene oxide and Eudragit® [12,13]. Additionally, these systems may be used for the local delivery of therapeutics to wounded oral tissues such as those suffering OLP and/or RAS [5] Several methods of polymer processing have been used including solvent casting, hot melt extrusion, advanced 3D printing techniques, electrospinning and freeze-casting [14,15]. Electrospinning is a cost effective and convenient way of producing nanofibrous samples with extremely high surface area to volume ratios which is particularly advantageous in drug delivery applications. The controllable high porosity of these materials ensures drug diffusion and mass transfer can be precisely controlled. The electrospun mats can be directly applied to the delivery site to provide a high local concentration of drug whilst minimising the systemic side effects. Recent advances in advanced electrospinning setups allow for the spinning of multi-drug solutions within a single fibre, allowing simultaneous delivery, enabling complex therapeutic treatment regimens [16].

One class of polymers which have been investigated for electrospinning are polyhydroxyalkanoates, which are produced as an energy store during the fermentation of microorganisms under nutrient limiting conditions. These polymers demonstrate remarkable biocompatibility with a range of cell types making them appropriate for biomedical applications [17–19]. The properties of these polymers depend greatly on the fermentation conditions such as microorganism species, nutrient availability, carbon source, and environmental conditions [20]. Typically, they can be classified depending on the number of carbon atoms in their monomer chains, short chain length PHAs, such as P(3HB) having 3-5 carbon atoms (scl) whilst medium chain length PHAs (mcl) contain 6-14 carbon atoms per monomer unit. Due to differing properties of scl-vs mcl-PHAs they have been applied to different scenarios in biomedical applications. The stiff and brittle properties of scl-PHAs mean that they lend themselves as materials for hard tissue engineering whilst the soft and flexible nature of mcl-PHAs make them more suitable for soft tissue applications [21]. During the electrospinning process it is necessary to blend the two as mcl-PHAs typically have low melting temperatures and bulky side chains which prevent the necessary polymer chain entanglement required for the formation of distinct and stable fibres [22]. We previously optimised the electrospinning of mcl-PHA-P(3HB) blends to ensure the correct mechanical properties for application to oral mucosal tissues [23]. In the current study, we aim to further modify the electrospinning process to provide a gradient style loading of clobetasol propionate (CP) throughout the scaffold architecture enabling the spatial delivery of CP in the direction of the OLP lesion. Additionally, we incorporated fluconazole (FLU) as a preventative to the secondary fungal infections often associated with treatment using steroid based formulations.

2. Materials and methods

2.1. Materials

CP powder, ≥98%, was purchased from Cambridge Bioscience (Cambridge, England, UK). FLU powder, 98%, phosphate buffered saline tablets (PBS), chloroform, ≥99.5%, dimethylformamide, ≥99.5%, methanol (MeOH), trifluoracetic acid (TFA) and acetonitrile (ACN) were procured from Fisher Scientific (Loughborough, England, UK). Defined Keratinocyte SFM, TrypLE express, MTT reagent, Penicillin-Streptomycin, 10,000 U mL^{-1} and Applied Biosystems™ SYBR™ Green Universal Master Mix were obtained from Thermo Fisher Scientific (Life Technologies) (Massachusetts, US). Methylene Blue, ≥82% dye content, Rhodamine B solution, 0.2% in isopropanol, Lipopolysaccharides (LPS) from *E. coli,* BioXtra, and primer sequences were purchased from Sigma-Aldrich (Gillingham, UK). TriPure and Transcriptor cDNA synthesis kit were purchased from Roche, (Roche Holding AG, Switzerland).

Medium-chain-length PHA was produced using bacterial fermentation technique with Gram negative bacterium (commercially sensitive) and purified as previously reported [19]. The short-chain-length PHA (poly(3-hydroxybutyrate) was produced using a Gram negative bacterium (commercially sensitive) using the parameters described in our previous publication [23].

2.2. Electrospinning for a gradient drug loading

An in-house electrospinning system was used to produce nanofibrous membranes, consisting of a high voltage source of maximum output 30 kV, 2 syringe drivers, a flat grounded collecting plate and a customised tubing system to allow concurrent injection of different polymer-drug solutions for creation of the gradient loaded membrane, as described in Fig. 1.

Polymer solutions for electrospinning were made based on preliminary studies into the optimal drug loading to ensure biocompatibility with oral epithelial cells, [23]. Briefly, 10% (w/v) polymer solutions were made using an 80:20 ratio of mcl-PHA:P(3HB) by first dissolving the P(3HB) in 90% of the final solvent volume via stirring with a magnetic stirrer. The mcl-PHA was then added to the solution and fully solubilised. Drugs were solubilised in the final 10% of the total solvent volume and added to the polymer portion of the solution. The

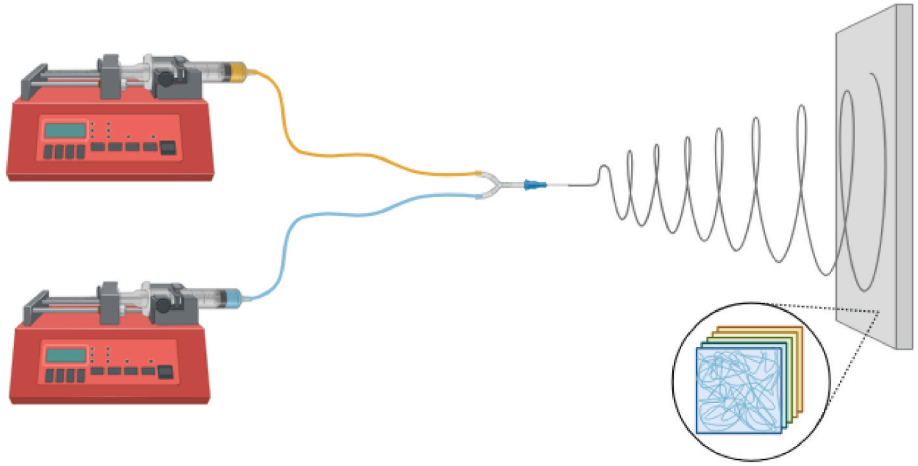


Fig. 1. Summarising the electrospinning setup used for the fabrication of gradient loaded electrospun samples where one syringe is filled with the polymer solution containing FLU only and one with polymer solution containing FLU and CP. Tailoring of the flow rates allows the creation of the gradient loading effect in 5 layers as shown and described in Table 1.

Table 1
Flow rate variation details used during the manufacture of gradient electrospun (ES_G) samples.

Time/ hr	Layer Number	Syringe 1 Flow Rate/mL/hr (FLU & CP solution)	Syringe 2 Flow Rate/mL/ hr (FLU solution)
0-0.4	1	0	1
0.4-0.8	2	0.25	0.75
0.8-1.2	3	0.5	0.5
1.2-1.6	4	0.75	0.25
1.6-2	5	1	0

solvent used was a 9:1 (v/v) mixture of $CHCl_3$:DMF.

Two different drug solutions were produced, one containing FLU only at a final concentration of 10%, in relation to the polymer mass in solutions. The second solution contained both FLU and CP at final concentrations of 10% and 2% respectively in relation to the polymer mass in solutions. The concentrations used for drug loading were determined based on the following rationale. Whilst CP is most routinely prescribed as a 0.05% ointment, the selected concentrations were informed by the literature on similar dosage forms to our proposed patches, which reported the use of 26.6 mg/mL, as well as by our previous optimisation experiments. [23,24]. The FLU dosing was decided based on similar rationale, [25–27].

Each polymer-drug solution was loaded into a separate syringe and connected to the Y-shape tubing system at the 2 inlet ports and the outlet port was then connected to a 21G blunt needle tip. This complete setup is shown in Fig. 1. Overall flow rate was maintained at 1 mL/h, a positive voltage of 15 kV was applied to the needle tip, and a distance of 15 cm was maintained between the needle tip and grounded collector. Flow rate for the evenly loaded samples (ES_E) was maintained at 1 mL/h overall by setting the flow rate of each individual syringe driver to 0.5 mL/h and spinning until 2 mL of solution was dispensed. The flow rates for gradient loaded samples (ES_G) are summarised in Table 1 as these varied over time to create the gradient effect in 5 different layers. Control electrospun samples were made using the polymer solution with no drug loading, under the same conditions.

2.3. Fibre characterisation

2.3.1. Scanning electron microscopy (SEM)

All images were collected using the Sigma 300 VP system (Zeiss, Germany). Prior to imaging samples were coated with a thin layer of Au-Pd using a sputter coating equipment, Polaron E5000 (Quorum Technology, UK) at 30 mA for 90 s under vacuum. SEM images were collected using secondary electron detection, at an accelerating voltage of 5 kV and a working distance of 7-8 mm.

2.3.2. Confocal imaging

To visualise the separation of the layers, fluorescent dyes were used. To the solution containing 10% FLU methylene blue was added and to the fibres containing both 10% FLU and 2% CP rhodamine was added. The electrospinning process was conducted as described above for the ES_G samples. The membrane was then snap frozen in liquid nitrogen and the cross-section was imaged using the confocal microscope (Aurox, UK) at excitation wavelengths of 405 nm and 550 nm.

2.3.3. Dynamic mechanical analysis (DMA)

Mechanical testing was performed using a DMA 850 (TA Instruments, Delaware, US). Analyses were performed under 3 different conditions: dry conditions at room temperature, 2) dry conditions at 37 °C and 3) submerged conditions (PBS) at 37 °C. The different testing conditions were investigated to ensure mechanical integrity during manufacture, storage and time of application as the manufacture and storage are under dry ambient conditions whilst the application is in a moist environment at body temperature of 37 °C. Rectangular specimens were cut to dimensions of 50x5x0.1 mm (lxwxh)and stored in a desiccator until testing. The testing was conducted as a rate-controlled strain ramp of 1 mm/min. Young's modulus was calculated as the gradient of the linear elastic region of the stress/strain curve.

2.3.4. Fourier transform infrared spectroscopy (FT-IR)

FT-IR spectra were obtained using the PerkinElmer Spectrum One spectrometer (PerkinElmer Ltd, Specac Ltd., Orpington, UK) with diamond window. Samples were analysed in the 4000-600 cm^{-1} wavenumber range, spectra were acquired at a resolution of 2 cm^{-1} and data presented is baseline corrected and normalised by maximum point in the system software, Spectrum v 5.0.1 (PerkinElmer Ltd, Beaconsfield, UK).

2.4. Drug release studies

2.4.1. Directional drug release

Drug release studies were performed in PBS release media under sink conditions at 37.0 ± 0.5 °C in a shaking incubator set to 100 rpm. Scaffolds were cut to shape in triplicate for each sample group, and mass was recorded giving a range of 50-70 mg. Samples were placed top down in a transwell insert for 6 well plate with 4 mL of release media below the transwell insert and 4 mL of release media above the transwell insert. This setup was used to allow the determination of the spatial release of

CP and FLU and is depicted in Fig. 2. At predetermined time points 0.4 mL of sample was withdrawn from both below and above the transwell insert and replaced with fresh release media. Both CP and FLU were quantified in each withdrawn volume using the following HPLC method.

HPLC analysis was carried out on an Agilent Technologies 1100 Infinity compact LC Series (Agilent Technologies, Cheshire, UK). A Zorbax LC, C18 reverse phase column with 5 μm particle size and dimensions of 250 × 4.6 mm was used. The separation of analytes was done at 24 °C in mobile phases composed of 0.1% TFA in water and 0.1% TFA in ACN. Conditions were as follows; 35% of ACN in water for 5 min at a flow rate of 0.6 mL/min, the flow rate was then increased to 1 ml/min between 5 and 6 min, finally the mobile phase composition was ramped to 100% ACN (+0.1% TFA) between 5 and 15 min at 1 mL/min. The conditions were then held as such until 20 min. UV signal was measured using an Agilent G1315A DAD detector at 250 nm. For each concentration, single injections of 20 μL were analysed [28].

Cumulative drug release was calculated above and below the transwell insert to show the directional release of the CP and FLU from both the evenly loaded (ES_E) and gradient loaded (ES_G) sample groups.

2.5. Biological characterisation

2.5.1. MOE-1a cell viability

Mouth ordinary epithelial cells (MOE-1a) were grown and maintained in defined keratinocyte serum free media (KSFM) supplemented with the KSFM growth supplement and 1% penicillin-streptomycin. Normal cell culture conditions were maintained during all biological studies of 5% CO_2, and 37 °C. TrypLE express was used for passaging when cells reached 70-80% confluence.

Cell viability was analysed using 3-(4,5-dimethylthiazol-2-yl)-2,5-diphenyl tetrazolium bromide (MTT). For this study MOE-1a cells were seeded at a density of 5×10^4 cells/mL in 12-well plates and allowed to attach overnight. Samples were washed with PBS, fresh media added and electrospun samples introduced (ES_CON, ES_E and ES_G). For the viability study the indirect transwell setup was chosen to ensure mechanistic clarity, this setup separates the material from the cells but allows soluble factors to diffuse. Therefore, the cytotoxicity caused by released drug or leachables from the scaffold are analysed rather than the direct effect of physical contact with the cells. Positive control samples (cells cultured in complete growth media with no electrospun patch or drug treatment), control electrospun samples with no drug loading, and negative controls (lysed with triton x-100) were included at each time point. Plates were incubated for 1, 3 and 7 days with media aspirated and replaced at day 3.

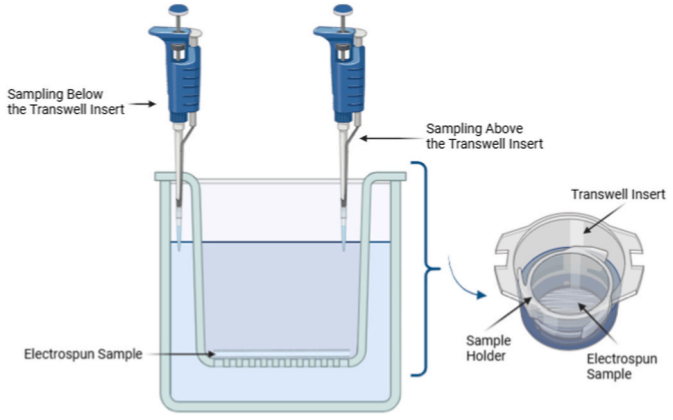


Fig. 2. Transwell setup for directional drug release analysis, electrospun samples are cut to size and placed in the transwell insert with a sample holder to prevent sample floating and prevent backflow of release media. At each time point samples are taken from both above and below the transwell insert to allow the analysis of the directional drug release of samples.

At each time point MTT solution (5 mg/mL in PBS, filter sterilised) was added to a final concentration of 0.5 mg/mL and incubated at 37 °C for 2 h. Culture media was removed and 500 μL of solubilisation buffer added (20% w/v SDS prepared in a 1:1 ratio of DMF: deionised water, pH adjusted to 4.7 using acetic acid). Samples were briefly agitated in the dark until complete solubilisation and then 100 μL aliquots were transferred in triplicate to a 96 well plate and absorbance was read at 572 nm using a microplate reader (Tecan, Switzerland).

Cytotoxicity was assessed using CyQUANT™ LDH Cytotoxicity Assay (Invitrogen, US), was used. The assay was used as recommended by the manufacturer, briefly, at each time point 50 μL of sample media was transferred to a 96 well plate and 50 μL of reaction mixture was added. Plates were incubated at room temperature in the dark for 30 min before adding the stop solution. Absorbance was measured at 490 nm with a background absorbance measured at 680 nm. Results reported are the difference between the two readings minus a media only control as a background LDH correction. The positive controls for this experiment were MOE-1a cells grown on standard cell culture treated plates and lysed using triton x-100 and negative controls were those grown on standard cell culture treated plates with no treatment.

2.5.2. In vitro wound healing study

The wound healing assay was carried out using the 4-well silicone culture inserts available from Ibidi (catalogue number – 80469). Inserts were placed in 12-well plates and cells seeded at 2.5×10^5 cells/mL with 100 μL per well. Plates were incubated overnight until confluent and then the silicone inserts were removed, leaving behind the cell free wound gap area. Samples were washed gently in PBS and complete growth media was added to the wells, patches in experimental groups were added in transwell inserts to give the following groups.

- Positive Control, complete growth media
- Control scaffold (ES_CON), electrospun sample with no drug loading
- Evenly loaded scaffold (ES_E), electrospun sample with uniform CP and FLU loading
- Gradient loaded scaffold (ES_G), electrospun sample with gradient CP and FLU loading

Following the removal of the silicone well inserts each sample was imaged at 0 h using light microscopy at 4 defined points. Samples were then returned to the incubator and at predefined timepoints samples were removed and imaged to allow for continuous monitoring of the wound closure. To facilitate imaging, at each timepoint the transwell insert containing the electrospun samples were removed using forceps and retained to be replaced following imaging. Samples were imaged at the same positions as the locations marked at T0, 0 h. Following image collection analysis was conducted using Image-Pro v11 software with the wound healing protocol, available in the cell biology plus package. All groups were run in triplicate with 4 analysis regions on each sample.

2.5.3. Inflammatory stimulated in vitro wound healing study

The study described above was repeated with modification to induce inflammatory expression in the MOE-1a cells. The same methodology was used, however after removing the silicone well inserts and washing in PBS the media introduced contained LPS from *E. coli* at a concentration of 10 μg/mL. This concentration was chosen due to reported concentrations used across the literature for use with various cell lines and a pre-screening of 0.1, 1 and 10 μg/mL LPS with the MOE-1a cells, investigating the expression of inflammatory markers at 24, 48 and 72 h post treatment (data not shown). The below conditions were set up to ensure inclusion of the appropriate controls required for the study.

- PC = Positive Control, cells only (Complete KSFM Media, -LPS)
- NC = Negative Control, cells only (Complete KSFM Media, +LPS)
- ES_CON = Electrospun Control (Complete KSFM Media, +LPS)

- ES_E = Evenly Loaded Electrospun (Complete KSFM Media, +LPS)
- ES_G = Gradient Loaded Electrospun (Complete KSFM Media, +LPS)

2.5.4. RT-qPCR

Sacrificial samples were set up as above to allow RNA extraction at time points of 6, 12 and 30 h of healing. At each time point media was aspirated and the cells lysed using TriPure Isolation Reagent. RNA was isolated following manufacturer's instructions, briefly to 1 mL of cell lysate 200 μL of molecular grade chloroform was added. The sample was homogenised and incubated at room temperature for 15 min before centrifuging at 12,000 g for 15 min at 4 °C. The upper aqueous phase was transferred to a clean Eppendorf and incubated with 0.5 mL ultrapure isopropanol for 10 min. The sample was centrifuged at 12,000 g for 10 min at 4 °C, resulting in the RNA pellet. The supernatant was discarded and the pellet washed in 75% ultrapure ethanol in molecular grade water. Following centrifugation at 7500 g for 5 min the supernatant was again discarded and any remaining ethanol allowed to evaporate, the pellet was then resuspended in TE buffer. RNA purity and concentration as analysed using a NanoQuant plate in a Tecan plate reader (Tecan, Switzerland).

Reverse transcription to cDNA was completed using the Transcriptor First Strand cDNA Synthesis Kit and used as advised by the manufacturer. In a reaction tube the following components were added to a total volume of 13 μL, 1 μg total RNA (variable volume), random hexamer primers to a final concentration of 60 μM (2 μL) and molecular grade water (variable volume, to make final volume of 13 μL). RNA secondary structures were denatured via heating at 65 °C for 10 min in the Thermo Hybaid PCR Express (Thermo Fisher, Massachusetts, US). To this tube the remaining components were added, Reaction Buffer (5x conc, 4 μL), RNase Inhibitor (0.5 μL), Deoxynucleotide Mix (2 μL) and Transcriptor Reverse Transcriptase (0.5 μL). The tube was returned to the thermal block and heated at 25 °C for 10 min followed by 55 °C for 60 min. For long-term storage cDNA was diluted in TE buffer and stored at −20 °C.

The gene expressions of inflammatory and wound healing related markers were determined with the SYBR Green PCR reagent kit using the Applied Biosystems 7300 Real-Time PCR System. Sequences of the primers used throughout the study are shown in Table 2 below. Gene expressions are normalised to GAPDH and ct values were analysed with the DataAssist V3.01 software and the fold change in gene expression calculated using the ΔΔct method.

2.6. Statistical analysis

Statistical analysis was carried out on data where possible. Mean values are presented as mean ± standard deviation. Statistical significance of appropriate data was tested by one way analysis of variance (ANOVA) with post-hoc Tukey's multiple comparison test and unpaired *t*-test. All data and statistical analysis were conducted using GraphPad Prism 10 software (GraphPad Software, Inc. USA). Confidence intervals were set to 95% and notation used for statistical significance throughout is as follows; * = $P \leq 0.05$, ** = $P \leq 0.01$, *** = $P \leq 0.001$, **** = $P \leq 0.0001$.

Table 2
Primers used for PCR gene expression analysis.

Gene	Forward/Reverse	Primer Sequence (5′-3′)
GAPDH	Forward	CTCCTGCACCACCAACTG
	Reverse	ATGAGTCCTTCCACGATA
IL-1b	Forward	GGCTGCTCTGGGATTCTCTT
	Reverse	ATCGTGCACATAAGCCTCGT
IL-6	Forward	GTCCAGTTGCCTTCTCCCTGG
	Reverse	CCCATGCTACATTTGCCGAAG
NFκB	Forward	GCTTAGGAGGGAGAGCCCAC
	Reverse	AAACATTTGTTCAGGCCTTCCC
FGF	Forward	AAGCGGCTGTACTGCAAAAACG
	Reverse	CTTTGATAGACACAACTCCTCTC
TGFβ2	Forward	TCTAGGGTGGAAATGGATACACGAACC
	Reverse	TGTTACAAGCATCATCGTTGTCGTCG
Coll1a	Forward	CGGCTCCTGCTCCTCTT
	Reverse	GGGGCAGTTCTTGGTCTC

3. Results and discussions

3.1. SEM

Fig. 3 shows the morphology of the nanofibres under SEM observation, when electrospun using the optimised parameters for mcl-PHA/P (3HB) blends as previously reported [23], smooth, bead free nanofibres were obtained. There were no obvious morphological differences between the evenly loaded and gradient loaded samples. However, in both sample groups evidence of drug incorporation could be seen in SEM images on the fibre surfaces, seen at texture as compared to the smooth fibre surfaces of the control samples. Based on our previous studies this is evidence of the fluconazole incorporation, because of the concentration at which the fluconazole is loaded, the saturation point of the electrospinning solution is met and the drug precipitates from the electrospinning solution during the spinning process. This is contrary to the results shown previously in which no physical evidence of FLU incorporation was seen in SEM images [29,30]. This is perhaps because of the method of addition of drug. Other authors solubilised the drug in a greater proportion of the solvent solution before adding to the polymer portion of solution which may explain the differences in the way in which the drug incorporation presents.

3.2. Confocal microscopy

Confocal microscopy was used to visualise the distribution across the cross-section of the gradient electrospun samples. Solutions for electrospinning were prepared to include fluorescent stains proving the gradient distribution of the CP throughout the electrospun scaffold as shown in Fig. 4. It can be clearly seen that there is good spatial separation between CP + FLU and FLU only portions of the patch as we see the CP + FLU positioned to the top of the patch and the FLU only toward the bottom of the patch. This spatial separation is a step toward the potential for directional release of CP to ensure targeted treatment of chronically inflamed tissues.

3.3. DMA

To investigate the suitability of the samples for mucosal patch applications the elasticity was studied. These mechanical properties are essential to ensure the integrity of the patch throughout the application time. The oral cavity is a mechanically dynamic environment with daily activities such as mastication, speaking, and swallowing contributing to the forces experienced. The most frequent location of oral lichen planus is on the buccal mucosa, one of the lining mucosal surfaces of the oral cavity. Such areas are non-keratinised soft tissues with elastic properties to accommodate the movement of the tongue and jaw. Therefore, the material produced for application to the surface should be highly elastic under tensile stress. Mechanical tests were carried out under 3 different conditions to ensure suitability during production and storage (room temperature), at standard body temperature (37 °C) and under conditions mimicking the oral cavity (37 °C, under submersion). Results shown in Fig. 5 confirm that all samples presented with Young's modulus below 10 MPa under all the tested conditions. Typically, the incorporation of drugs into the electrospun fibres increased the Young's modulus from 3.862-4.22 MPa to 6.23-9.34 MPa dependent on the testing conditions. Modulus increases can be experienced due to restriction of polymer chain mobility due to interaction with drug molecules, enhanced structural order due to the presence of drugs or fibre reinforcement by the drug as opposed to showing plasticising effects [31–33]. Due to the hydrophobic nature of both the polymer and drugs used in this system, the two may mix more uniformly within the polymer

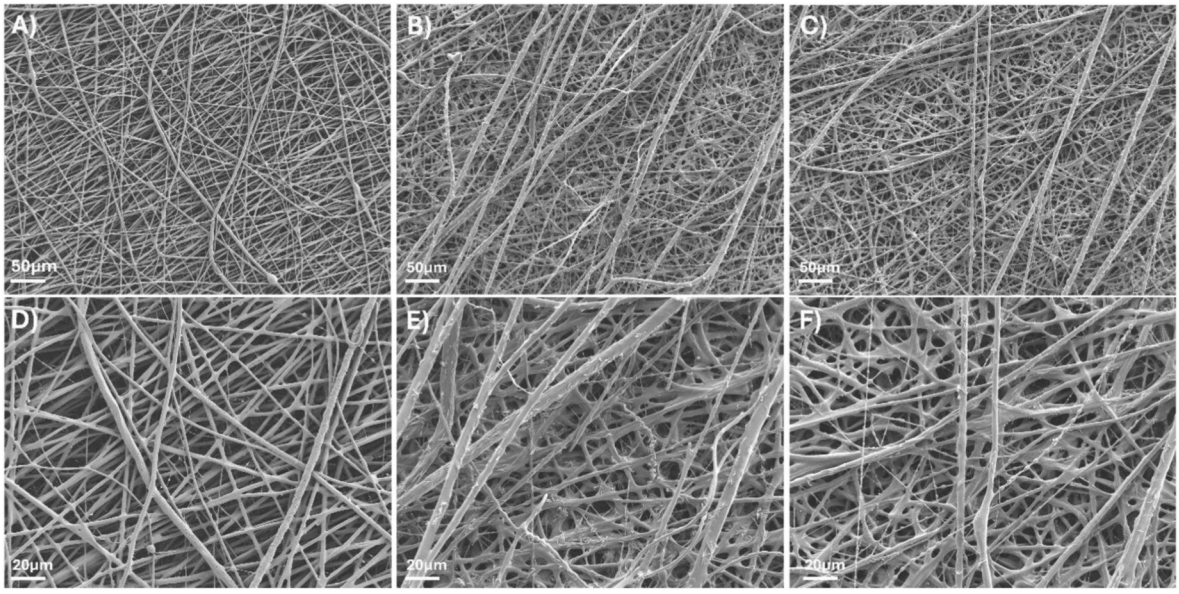


Fig. 3. SEM images showing the electrospun fibres produced using the dual input setup A&D) Fibres with no drug loading (ES_CON) B&E) Evenly loaded (ES_E) and C&F) Gradient loaded (ES_G). Where scale bars show 50 μm for A-C and 20 μm for D-E.

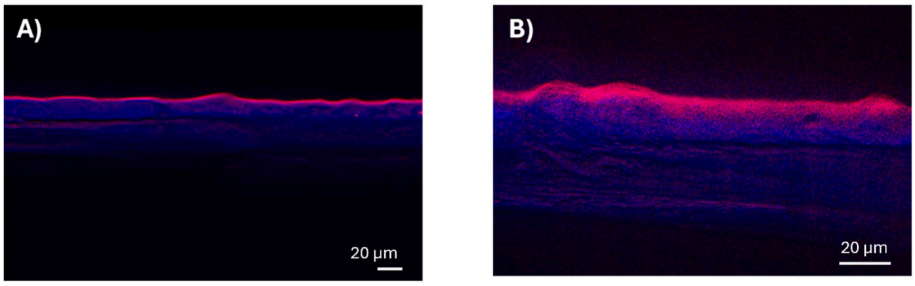


Fig. 4. Confocal microscopy images showing the distribution of FLU and CP throughout the cross section of the scaffold produced methylene blue stained fibres show the fibres composed of 80:20 mcl-PHA:P(3HB) + 10% FLU and rhodamine (red) stained fibres show the fibres composed of 80:20 mcl-PHA:P(3HB) + 10% FLU +2% CP. (For interpretation of the references to colour in this figure legend, the reader is referred to the Web version of this article.)

giving fewer phase-separated domains and more efficient stress transfer resulting in higher stiffness [34,35]. If the drug exhibits limited solubility within the polymer matrix, it may remain in crystalline/semi-crystalline state, acting like a filler in the electrospun fibres. Such rigid dispersions can act as filler-like inclusions thus increasing the modulus [36,37].

To ensure suitability of the scaffolds for use in soft tissue applications we are aiming to match the properties exhibited by the native tissue. However, it is difficult to define the exact values of Young's modulus for the oral mucosal tissues given the range of different anatomies within the oral cavity, the range of different types *in vivo/ex vivo* tissues tested and the many different testing methods used to assess the mechanical properties. Previous reports of the Young's modulus of oral mucosal tissues quote ranges between 0.91 and 11.12 MPa when tested in tensile strain [38], which suggests that the materials produced within this study have appropriate elastic properties for use in transmucosal drug delivery. Previous studies focusing on oromucosal drug delivery systems describe Young's modulus values of 2.18-3.082 MPa using chitosan-PVA electrospun fibres [39]. Whilst these values are lower than that seen in our study, elsewhere modulus values of 12-28.1 MPa were described by Olmos-Juste et al. for their 3D printed interventions [40]. Khan et al. described their film formulations of metolose containing 0 and 0.5% PEG plasticising agent to have the best mechanical properties for oromucosal applications, these formulations gave Young's modulus values of around 4 – 9 MPa [41]. Given the similarity of modulus values achieved within our study to those reported in the literature for both the native mucosal tissues and drug delivery platforms produced for similar applications, we believe the mechanical properties achieved here are appropriate for oromucosal drug delivery.

3.4. FT-IR

Chemical characterisation using FT-IR analysis was performed to investigate the functional groups of chemical interactions within the materials. Fig. 6 shows the FT-IR spectra for the samples before and after drug incorporation. The most intense peak is observed at 1724 cm^{-1} corresponding to the C=O carboxyl group vibration of the ester bonding in the polymer structure. This peak has been reported at slightly lower wavenumber of 1720 cm^{-1} for scl-PHAs (P(3HB)) [42], whilst for mcl-PHAs this peak is reported to lie closer to 1725 cm^{-1}, given the higher proportion of mcl-PHA in the electrospinning polymer blend this peak appears closer to that for mcl-PHA. Evidence of the P(3HB) can be seen throughout the spectrum, peaks at 1386 cm^{-1}, 1128 cm^{-1} and 721 cm^{-1} corresponding to -C-H bending, -C-O stretching and C-C bending of the SCL polymers crystalline phase respectively [43–45]. In the fluconazole spectrum shown in Fig. 6B vibration of the triazole ring was found at 1501 cm^{-1} whilst the peak shown at 1618 cm^{-1} was indicative of the C=C stretching bond, both of which are evidenced in the even (ES_E) and gradient (ES_G) loaded samples but not in the control electrospun patch. The absence of peaks relating to the CP

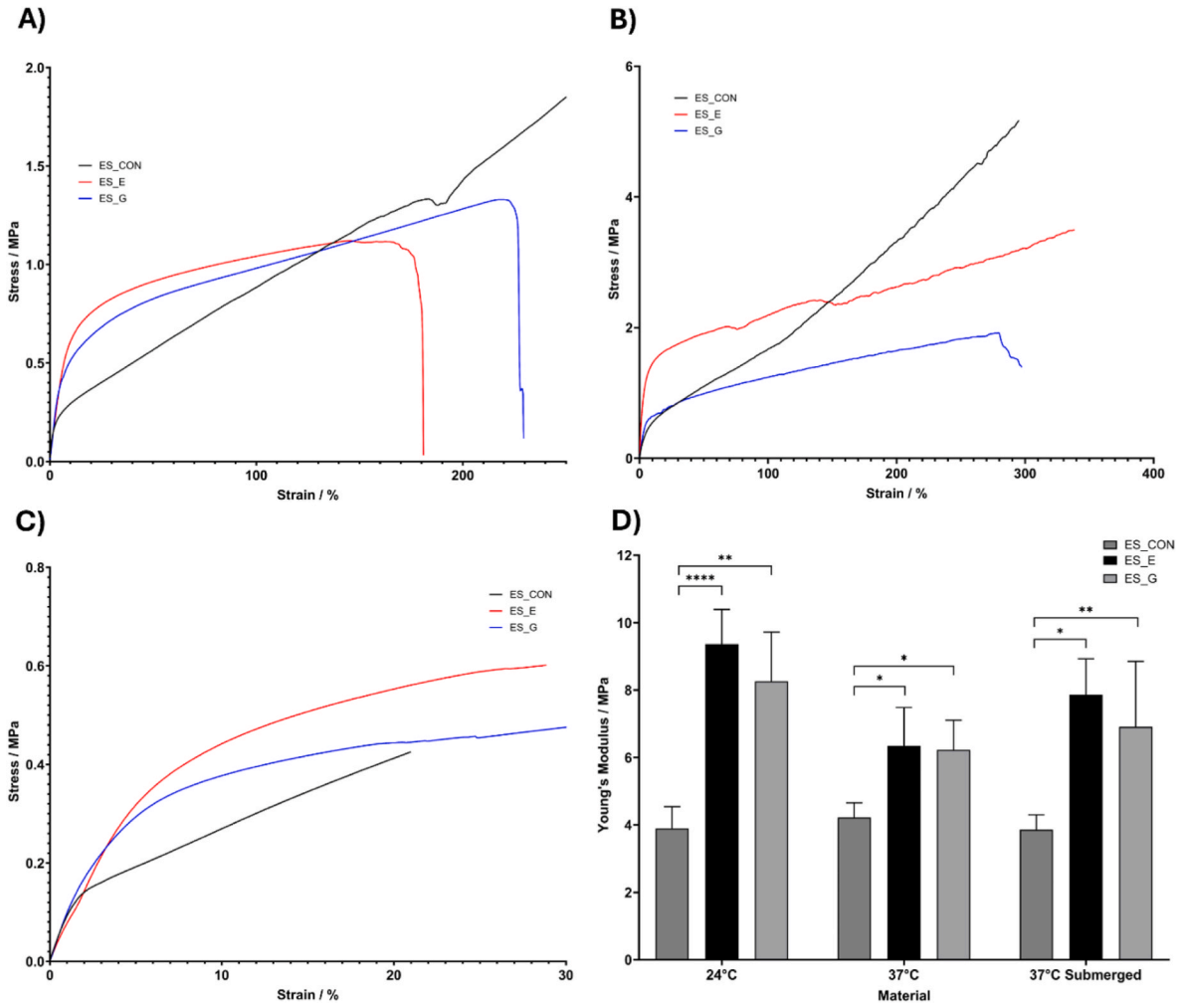


Fig. 5. Raw data Stress-Strain Curves showing mechanical properties of the control dual feed fibres (ES_CON), evenly loaded fibres (ES_E) and the gradient loaded fibres (ES_G) loaded fibres under 3 testing conditions **A)** ambient conditions **B)** at 37 °C and **C)** submerged in PBS at 37 °C **D)** Data analysis of Stress-Strain Curves showing Young's modulus of the control dual feed fibres (ES_CON), the even drug (ES_E) and the gradient drug (ES_G) loaded fibres under 3 testing conditions ambient conditions, at 37 °C and submerged in PBS at 37 °C.

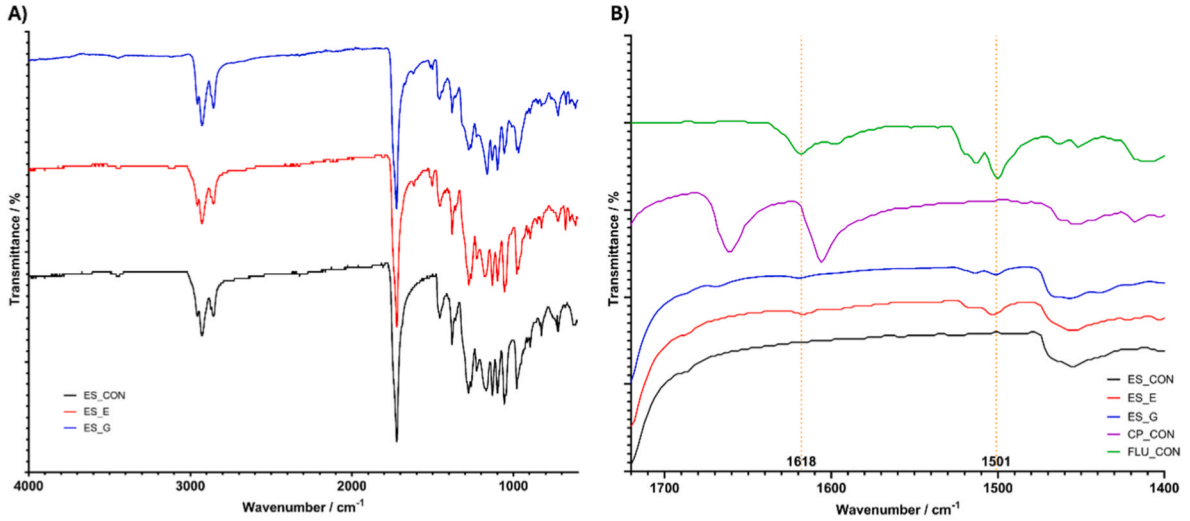


Fig. 6. A) FTIR spectra showing chemical properties of the control, even drug loaded and the gradient drug loaded fibres **B)** Showing relevant wave ranges to highlight the presence of CP and FLU in ES_E and ES_G samples.

incorporation is attributed to the low loading concentration of this drug and the overlap of potential vibrations for CP with the polymer

vibrational modes.

3.5. Drug release

The *in vitro* release profile from the mcl-PHA/P(3HB) electrospun fibres was assessed in PBS at pH 7.4 to evaluate the directional release from the even and gradient loaded scaffolds. The cumulative release of both CP and FLU from the drug loaded patches are shown in Fig. 7 both drugs show a sustained release up to 8 h *in vitro*, ensuring an appropriate dosage delivery for the duration of patch application.

Fig. 7A shows the cumulative release of CP from both evenly loaded and gradient loaded patches. It is clear from this release profile that the CP release on each side of the patch differs between the two groups. The evenly loaded patches (ES_E) show comparable release in both directions whereas the CP release from the gradient loaded patches (ES_G) shows a clear bias in CP release above the transwell insert in the direction of the CP loaded area. There is a very limited amount of CP release from the ES_G sample in the direction of the side of the sample which has no CP loading. We hypothesise that this is because of the interconnected porous nature of electrospun scaffolds, allowing some backflow of released drug [46]. However, we expect that this is still a significant improvement over current treatment therapies which show significant clearance with retention times of only minutes, typically less than 1 h [47]. It is difficult to define the exact retention of drug at application sites in these scenarios and not many in depth studies investigate this. However, one study utilising a water-soluble steroid to investigate drug uptake at oral application sites showed poor retention in most cases with the palatal, buccal and sublingual mucosa showing 9.9%, 24.1% and 65.4% retention respectively [48]. This study gave solid evidential links between application site dependency and unintended contact and given that the majority of OLP is observed on the buccal mucosa it is likely that close to 75% of applied formulations to treat OLP lesions are lost because of salivary washout [49].

When investigating the mechanisms of drug release using various fitting models the best fit release models differ between the sampling done above the transwell in comparison to below the transwell. Samples taken from above the transwell, near the CP rich region, showed a best fit to the zero-order release mechanism whilst the release to the chamber below shows closest fit to the Higuchi model (Table 3). These release profiles make sense for the system we have engineered. In the upper chamber a constant release rate over time is achieved due to a maintained concentration at the material-media interface. The drug-flux is remaining constant hence showing apparent zero-order kinetics [50].

Table 3
Showing calculated r^2 values for CP and FLU release from the ES_E and ES_G patches as calculated from zero order, first order and Higuchi release models.

	Zero Order		First Order		Higuchi	
	CP	FLU	CP	FLU	CP	FLU
ES_E Above	0.981	0.946	**0.991**	**0.983**	0.883	0.945
ES_E Below	0.985	0.961	**0.989**	**0.987**	0.861	0.921
ES_G Above	**0.995**	0.979	0.977	**0.984**	0.845	0.859
ES_G Below	0.837	0.982	0.852	**0.984**	**0.968**	0.846

Conversely the release rate in the other direction is slowing down over time, this is most likely because the CP must diffuse across a greater thickness of the material prior to interacting with the material-media interface. Additionally, the area from which this drug originates is a lower concentration region than that of the upper sampling chamber. These phenomena are consistent with the Higuchi model where the rate of release is dependent in the square root of time [51].

The FLU release, Fig. 7B, however is comparable in both directions across both the evenly loaded and gradient loaded sample groups. These results verify that the dual input electrospinning system for manufacturing the gradient loading successfully incorporated spatially separated drug loading with the ability for directional drug release. Under all conditions the first order release rate best fitted the profile shown by the FLU indicating that the release rate is concentration dependent with the amount of drug released being proportional to that remaining in the patch. Since a portion of the drug in this system is located at/near the fibre surfaces upon contact with surrounding medium the surface-associated drug dissolves quickly. This establishes a concentration gradient between the fibre interface and surrounding medium. As the release continues the remaining drug available near the surface decreases, proportionally reducing the dissolution rate. The rate of release is therefore dependent on the amount of drug remaining in the system which is consistent with the first-order ki [1]. Severa.

3.6. Cell viability and cytotoxicity

To study the cytocompatibility of the patches MOE-1a cells were used in the MTT and LDH assays. Results of cell studies are shown in Fig. 8. These assays have shown no indication of reduced viability with all timepoints having comparable percentage viability between positive controls and electrospun samples, both controls and drug loaded. The LDH assay results complement those of the MTT assay as there are no

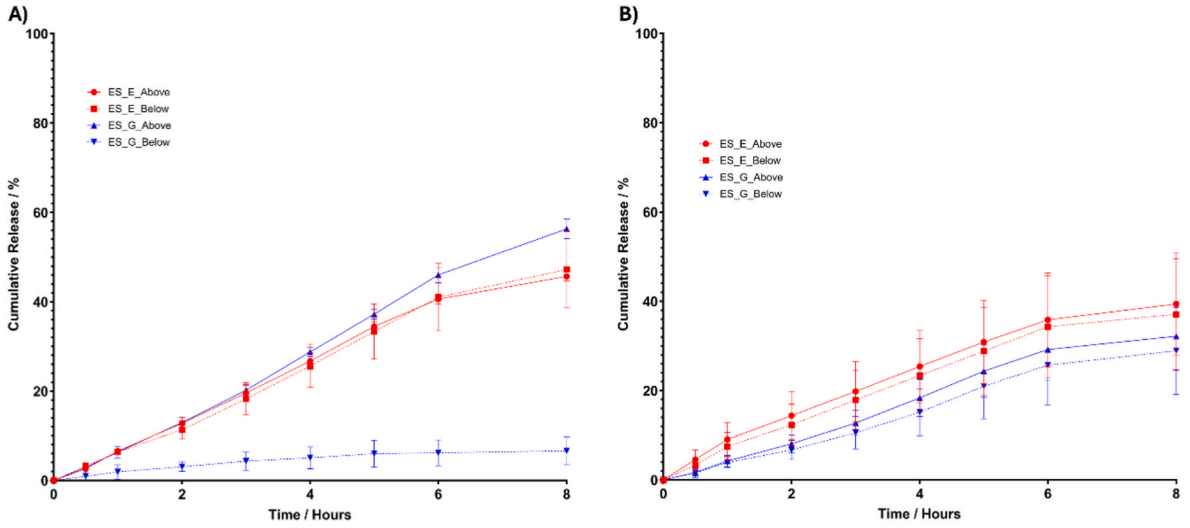


Fig. 7. Percentage cumulative release of **A)** CP and **B)** FLU from the evenly and gradient loaded electrospun scaffolds above the transwell insert (solid lines) and below the transwell insert (dashed lines).

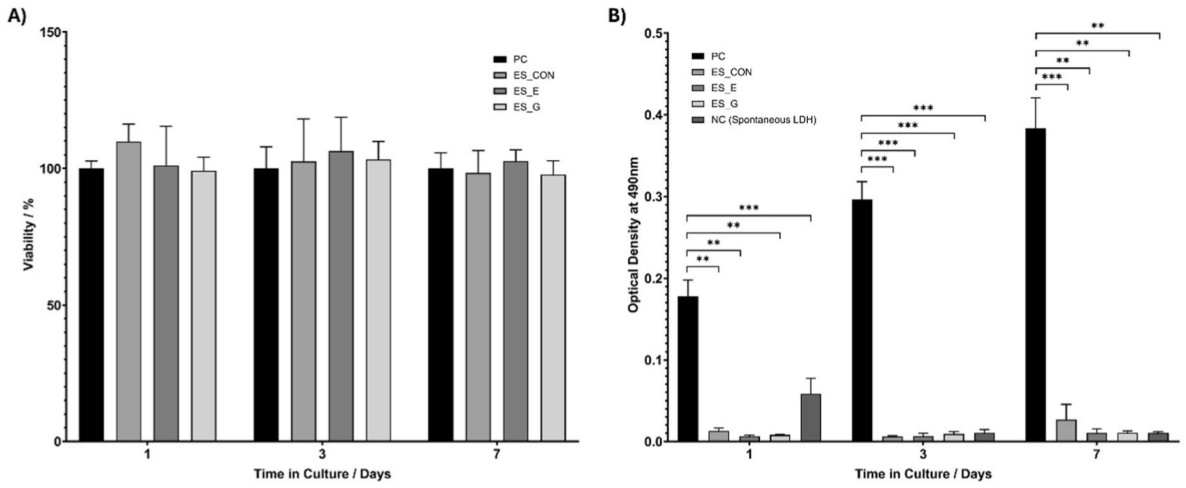


Fig. 8. A) MOE-1a viability measured using the MTT method and **B)** Cytotoxicity measured using the LDH assay for cells cultured in the presence of the control (ES_CON), evenly loaded (ES_E) and gradient loaded (ES_G) electrospun patches.

significant increases in absorbance from the spontaneous LDH release to the samples containing the electrospun samples. The increase in absorbance in the LDH assay over the 7-days is normal as a consequence of cell turnover in culture.

The cytocompatibility of native mcl-PHAs have been investigated for numerous tissue engineering applications spanning neural, cardiac, musculoskeletal and dermal targets [17,18,52–54]. We previously reported the cytocompatibility of the electrospun mcl-:scl-PHA blends loaded with either CP or FLU with MOE-1a cells, optimising the drug loading concentration to ensure appropriate compatibility [23]. Within the current study we have confirmed that there is no adverse effect because of pharmacological compounding of the two within the ES_E and ES_G samples. These results are encouraging for the scaffolds as oromucosal drug delivery devices and suggest that the controlled release rate of the CP is appropriate as high concentrations of corticosteroids are cytotoxic and this is not experienced in our model *in vitro* system. Similar cytocompatibility of CP loaded chitosan-gelatin based materials have been shown using THP-1 (monocytes) [55]. The same group have described the loading of electrospun scaffolds with similar concentrations of CP to that used in our study (2%) gaining exceptional cytocompatibility with THP-1 cells (>90%) for all formulations both with and without inflammatory activation [56]. A study incorporating up to 5% CP in PLA electrospun fibres has shown greater cytotoxicity to what we observed in our study [57]. This may be due to the base polymer in the patch material presenting with a higher cytotoxicity profile, approximately 20%, compared to the negligible cytotoxicity observed for the native mcl-PHA/P(3HB) controls (ES_CON) used for our formulation. Alternatively, the PLA formulation showed a significant burst release of CP compared to our mcl-PHA/P(3HB) based fibres which may also be contribution to the cytotoxicity experienced by Mazzinelli et al.

3.7. *In vitro wound healing studies*

The *in vitro* wound healing studies were conducted with and without LPS inflammatory stimulation. Initial studies without LPS stimulation confirmed that the drug incorporation did not cause any adverse effect on the rate of *in vitro* gap closure as shown in **SI1**. These results align well with the those obtained in the viability and cytotoxicity assays (Fig. 8) providing further confirmation that the combination drug loading is not adversely impacting the cytocompatibility of the fibres. The cytocompatibility was further confirmed during the initial *in vitro* wound healing study, which lacked LPS inflammatory stimulation, as there was no significant difference in the rate of wound gap closure between the positive control group and the groups containing electrospun samples. The omission of inflammatory stimulation in this model can explain the lack of expedited *in vitro* wound gap closure as the mechanism of action of CP, the drug to enhance the healing potential, is to block glucocorticoid receptors resulting in modulated inflammatory response at the wound site. In order to investigate this further this *in vitro* study was then conducted with inflammatory stimulation using LPS from *E. coli*, Fig. 9. The inflammatory stimulation of MOE-1a cells using LPS has been previously described [58]. In this model the drug loaded samples showed similar rate of epithelial migration to positive controls, whilst untreated negative controls stimulated with LPS showed significantly increased gap area remaining in comparison to ES_E and ES_G treated samples at 30 h (Fig. 9C).

In the inflammatory stimulated model, the inclusion of LPS caused a significant decrease in the rate of epithelial migration compared to the positive controls. These results agree with those reported by Yang et al. for IEC-6 (rat intestinal epithelial cells) in which LPS treatmenr notably inhibited the cell migration [59]. Similar effects have been shown using *in vivo* murine models, where LPS treatment significantly decreased wound healing rate and increased inflammatory cell infiltration in a skin wound model [60]. The control electrospun scaffolds with no drug loading did not enhance the rate of healing observed during inflammatory stimulation with the wound area remaining at 30 h being comparable to that of the negative, LPS treated controls. This confirms there are no innate anti-inflammatory effects of the native PHA in this model and the improvements observed in the rate of epithelial migration in this inflammatory stimulated epithelial model must be due to the incorporated drugs in the ES_E and ES_G sample groups. Similar effects on inflammatory stimulated models have been observed for chrysin loaded nanofibres using murine macrophage cells, J774A.1. Here, the inclusion of native PCL/PEG nanofibres did not reduce expression of inflammatory markers and cytokines but those containing chrysin did [61]. Elsewhere platelet-rich plasma infused nanofibres have shown the potential to modulate the level of pro-inflammatory markers in macrophage responses to stimulation with LPS compared to control unloaded nanofibre samples. The platelet-rich plasma nanofibres successfully decreased levels of IL-6 and TNF-α, whilst pro-healing factors such as TGF-β and IL-10 were upregulated [62]. However, these results were not compared to LPS deficient controls so it cannot be concluded to what extent the inclusion of the platelet derived factors restored normal functions.

Whilst these results are promising in relation to the potential for the patches produced to modulate inflammatory marker expression in an *in vitro* epithelial inflammatory model there are some limitations to the model for translation to *in vivo* OLP pathologies. Within our *in vitro*

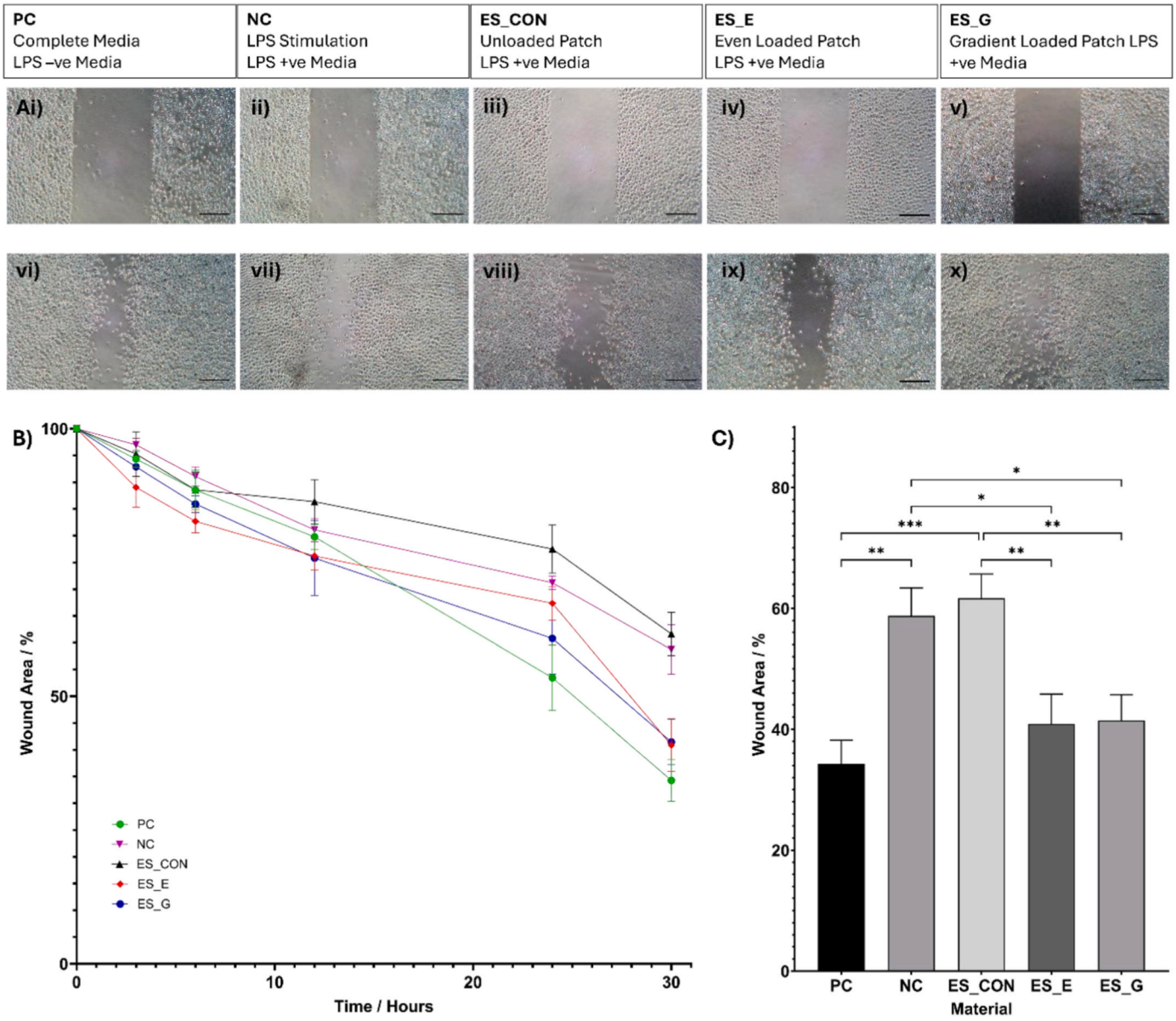


Fig. 9. A) Phase contrast images showing *in vitro* wound gap closure in an MOE-1a cell monolayer during treatment using the control and drug loaded electrospun patches in comparison to positive control, drug control and LPS stimulation groups. Time points show **(Ai-v)** T = 0, the penultimate time point at T = 30 h **(Avi-xi)** before full wound closure was seen in sample groups**. B)** rate of healing during stimulation with LPS from *E. coli* from 0 to 30 h **C)** The statistical analysis of the wound area at 30 h. Scale bar = 50 μm.

model to major limitations are the lack of complex chronic immune-cell infiltration such as the infiltration of activated $CD8^+$ T-cells characteristic of OLP disease state. Additionally, the complex microenvironment of the oral cavity is missed such as the multi-layered extracellular matrix, microvascular networks and multispecies oral microbiome. Future studies should move toward testing in a complex *in vitro* tissue model of OLP such as those outlined in the recent review by Jantakee et al. [63]. Eventually a suitable *in vivo* model such as the described lichenoid lesion models which clinically and/or histologically mimic OLP should be considered [64–66].

3.8. RT-qPCR

To further investigate the effect of the drug incorporation in fibres on the wound healing potential, RNA was extracted at set time points throughout the *in vitro* wound healing study to use for analyses of inflammatory and wound healing related gene expressions. In all cases the stimulation of MOE-1a cells with LPS induced the expression of inflammatory markers IL-1b, IL-6 and NκFB. Conversely the inclusion of LPS in the model significantly decreased the expression of wound healing markers at all timepoints. Interestingly, despite the lack of effect of the native electrospun scaffolds (ES_CON) on the rate of epithelial gap closure (Fig. 9), it seems that during the gene expression analysis some inflammatory markers could be downregulated in comparison to negative controls due to ES_CON inclusion. This was experienced for both IL-1b and NFκB expression during the study. The TLR4 signalling pathway is a key mediator of cell responses to LPS stimulation and it is possible that the inclusion of the mcl-PHA/P(3HB) blend, which is inherently hydrophobic, may interact hydrophobically with the lipid rafts causing interruption and interference with receptor clustering which is essential for the initiation of inflammatory pathways [67,68]. The idea that hydrophobic molecules can alter Toll-like Receptor 4 dimerization and the downstream cytokine production has been previously reported and it is possible that the hydrophobic nature of the mcl-PHA/P(3HB) and their

degradation products may exhibit similar effects [69,70]. Although, the potential for the polymer matrix to partially adsorb or sequester the LPS may offer an alternative explanation to the reduced expression of some of the proinflammatory markers during treatment with the native electrospun sample group. The adsorption of LPS by numerous polymers has been shown throughout the literature, usually in relation to nanoparticle systems, however there is reason to believe that the same effect could be experienced within our system [71].

The inclusion of the drug loaded scaffolds further reduced the expression of inflammatory markers at the 6-h timepoint, showing comparable expression to the positive controls in most cases (Fig. 10A–C). This is likely due to the mechanism of action of CP which uses glucocorticoid receptor-mediated interactions to downregulate NF-κB transcription leading to reduced production of cytokines such as IL-1b and IL-6. These conditions of inflammatory sequestering are reflected in our gene expression analysis results and may provide an explanation for the improved epithelial migration rate in the drug loaded sample groups. Similar results have been reported for the development of a multilayer patch containing CP which showed good cytocompatibility with THP-1 cells and described an improved anti-inflammatory efficacy of the patch-based system over free CP [55]. In a different nanofibre system, combining ethylcellulose/gliadin fibres with active ingredients of aloe vera, zinc oxide nanoparticles and mycophenolate mofetil demonstrated the potential to control the LPS induced expression of inflammatory markers by human gingival fibroblast cells [72]. Here, the inclusion of the active ingredients in the fibre formulation significantly reduced levels of TNF-α and IL-6 expression during LPS stimulation *in vitro*. Elsewhere, the inclusion of CP in electrospun mucoadhesive patches enabled the reduction of inflammatory IL-2 production by an *in vitro* oral mucosal tissue engineered equivalent which was stimulated using activated T-cells. The use of the patch successfully reduced IL-2 levels to a comparable level to that of a CP solution [73]. The improvements in the expression of inflammatory markers seen throughout the *in vitro* wound healing study during inflammatory challenge suggest that the patches produced in this study may have the potential to provide a solution which aids wound gap

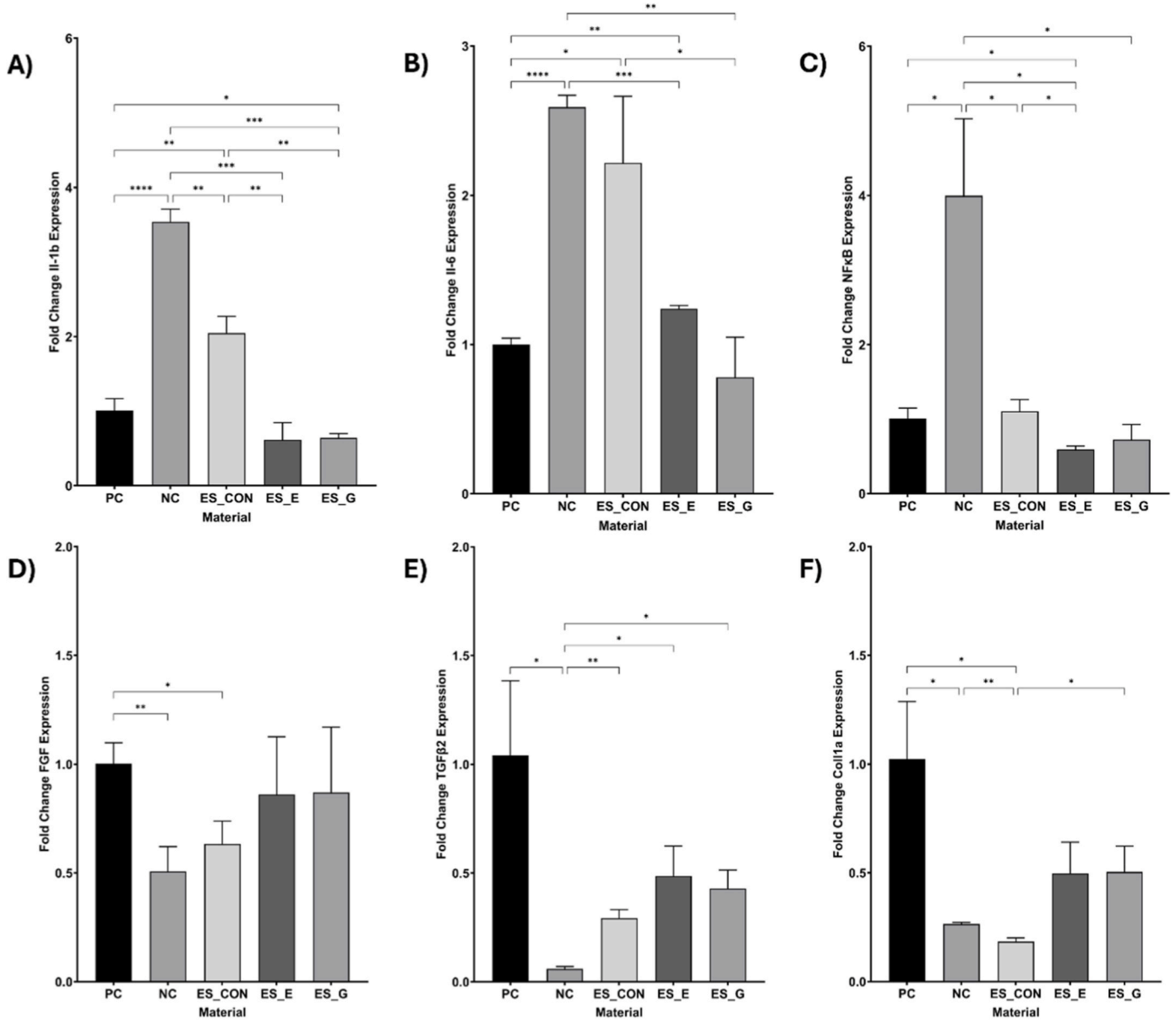


Fig. 10. A-C) Inflammatory marker **A)** IL-1b **B**) IL-6 and **C)** NFκB and **D-F**) Wound healing marker expression **D)** FGF **E)** TGFβ2 and **F)** Coll1a by MOE-1a cells during *in vitro* wound healing assay (6 h) after exposure to LPS from *E. coli* to induce inflammatory expression. Results are normalised to the expression of HKG GAPDH and fold change calculated using the ΔΔct method.

closure via suppression of the sustained inflammatory phases in conditions of chronic inflammation.

To assess the effect of the scaffold application on the expression of wound healing markers we considered FGF, TGFβ2 and Coll1a gene expression, during the inflammatory challenged *in vitro* wound healing model. Here we saw the significant reduction in expression of all markers at both time points during treatment with LPS (NC) in comparison to positive controls (Fig. 11). The suppression of these markers was most likely as a result of the changes in inflammatory marker expression shifting the signalling from a reparative functionality to a pro-inflammatory state. During this switching the inflammatory upregulation actively suppresses genes involved in tissue repair and healing. This inflammatory signalling may actively antagonise the TGFβ pathways rather than a passive mechanism of signalling disruption. As previously described the LPS activates a core inflammatory transcriptional response via TLR4, ultimately leading to the activation of NK-κB pathways. The activation of this pathway has several downstream consequences one of which is Smad7 induction, an inhibitory Smad which instead of propagating TGFβ signals in the way Smad 2 or 3 do, blocks them [74]. Smad7 typically interferes at the receptor level of signalling, binding to activated TGFβ receptor I and preventing the phosphorylation of Smad2 and Smad3. Eventually this can lead to receptor degradation because of ubiquitin ligases [75]. Overall, this mechanism prevents nuclear translocation for collagen and ECM protein transcription leading to weaker wound-healing phenotypes of cells which is also evident in our data showing suppressed collagen I expression following treatment with LPS (Figs. 10F and 11F). Additionally, the inclusion of LPS in systems is known to inhibit TGF-β signalling and suppress collagen synthesis via induction of ROS [76]. Whilst conflicting results can be found in the literature relating to the effect of ROS on TGF-β signalling, with some reports showing enhanced expression during ROS exposure [77]. This effect is extremely dependent on the ROS levels, the cell types studied, and the duration of exposure. In the context of this study, it is most common that ROS contribute to the suppression or dysregulation of TGF-β/Smad signalling [78,79].

At 6 h the expression of all wound-healing related markers

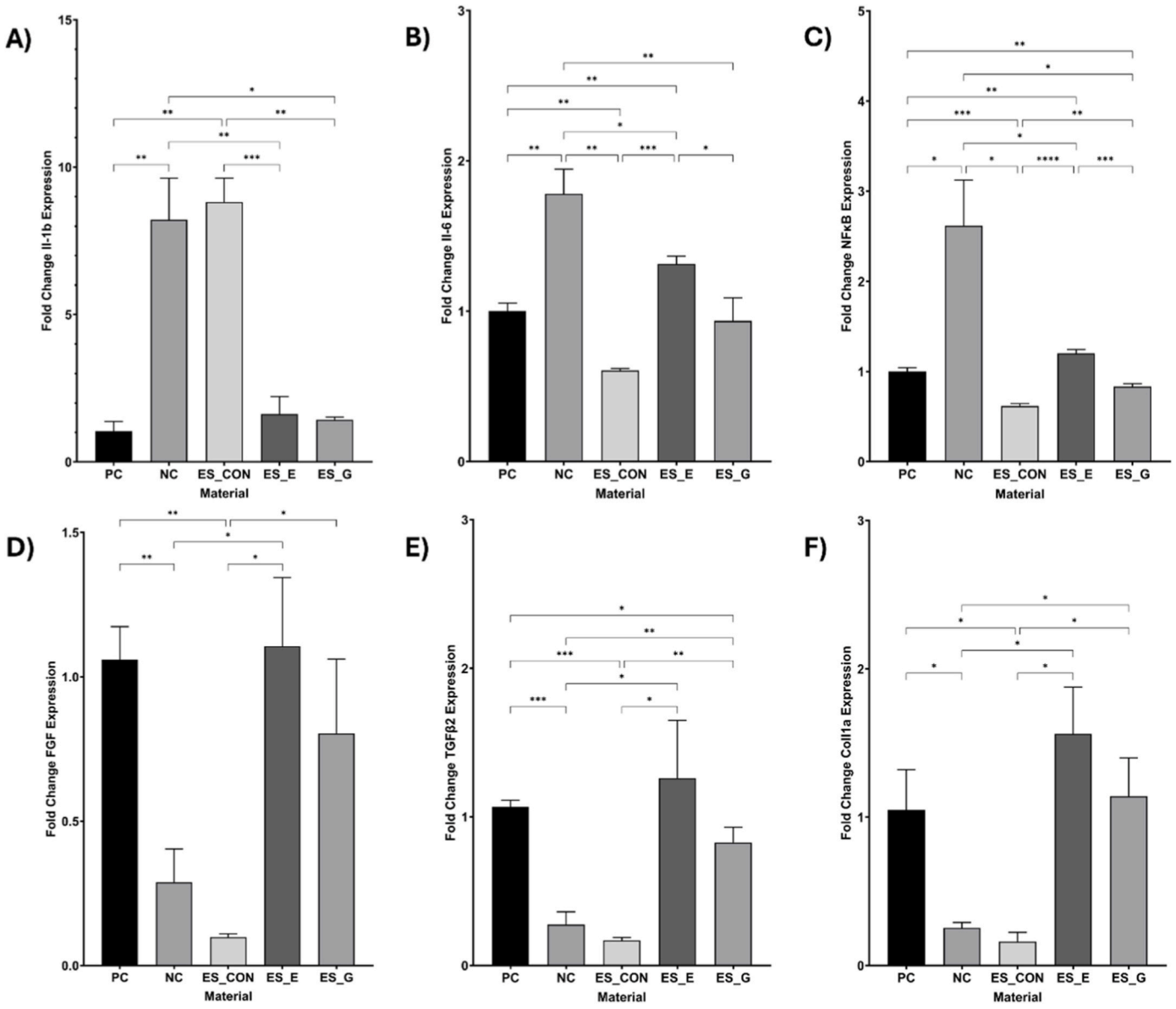


Fig. 11. A-C) Inflammatory marker **A)** IL-1b **B**) IL-6 and **C)** NFκB and **D-F**) Wound healing marker expression **D)** FGF **E)** TGFβ2 and **F)** Coll1a by MOE-1a cells during *in vitro* wound healing assay (12 h) after exposure to LPS from *E. coli* to induce inflammatory expression. Results are normalised to the expression of HKG GAPDH and fold change calculated using the ΔΔct method.

(Fig. 10D–F) was improved when exposed to the drug loaded electrospun samples (ES_E and ES_G) over that seen for the negative controls but only significantly so for TGFβ2. These results are plausible given the mechanism of action of CP which enables the suppression of the upstream inflammatory and oxidative pathways which are inhibiting the reparative signalling as previously described. At 12 h the treatment with the drug loaded electrospun samples continued to regulate the TGFβ2 expression whilst additionally restoring the levels of FGF and Collagen I expression. This delayed restoration of FGF and Collagen I expression compared to that of TGFβ is consistent with normal wound-healing biology. Given that TGFβ is an upstream regulatory signal whilst FGF and Collagen I are both downstream functional repair responses requiring transition out of the proinflammatory state induced by the LPS toward a proliferative, remodelling phase.

4. Conclusions and recommendations

Throughout this study we have shown the potential to simply modify electrospinning setups to produce gradient loaded scaffolds for spatial drug delivery. We characterised these patches for treatment of oral mucosal diseases. Our studies have shown the mechanical suitability of the scaffolds for use in oral applications and the ability to release drugs in a directional manner. Biological characterisation was completed using oral epithelial cells demonstrating no significant change in cell viability or cytotoxicity compared to the control electrospun samples, confirming the drug dosage was suitable to maintain cytocompatibility. Preliminary *in vitro* wound healing studies with LPS induced inflammatory stimulation and subsequent gene expression analysis showed that the introduction of the drug loaded samples to the system could successfully aid epithelial migration in an *in vitro* wound model. The qPCR analysis provides initial evidence that the improved wound closure was related to the altered inflammatory responses leading to downstream improvements in expression of wound healing markers. Given that there are some limitations with the current study, such as thorough evidence of improved wound healing under conditions of innate immunomodulatory chronic inflammation, future studies should focus on the development of 3D tissue models of oral injury with the inclusion of immune cells and relevant *in vivo* models to further elucidate the mechanism of action. Additionally, the level of anti-fungal activity achieved by the FLU inclusion is not described in this manuscript and should be investigated. The current patches are not optimised to ensure adhesion under wet conditions and given that the end application in the oral cavity is reliant on mucoadhesion, strategies should be investigated to ensure appropriate levels of mucoadhesion can be achieved. This may involve the application of a coating layer using materials such as polydopamine, Carbopol or chitosan which are known to enhance adhesion under wet conditions. The mucoadhesive properties should then be tested using *ex vivo* mucosal tissues to ensure that clinically relevant results can be obtained.

This developmental study has provided a basis suggesting that the electrospun patches investigated here have appropriate physicochemical and mechanical properties and may be useful in the treatment of oral lichen planus. The positive results obtained should be used as a guide to further investigate the potential these patches have in the treatment of oral lichen planus. Future studies should focus on investigation and enhancement of the mucoadhesive properties and more advanced and clinically relevant *in vitro* and *in vivo* studies to confirm and elucidate the mechanisms behind improved wound healing characteristics.

CRediT authorship contribution statement

Robyn A. Macartney: Writing – review & editing, Writing – original draft, Methodology, Formal analysis, Data curation. **Harshavardhan Budharaju:** Writing – review & editing, Writing – original draft, Methodology, Investigation. **Andrew M. Smith:** Writing – review & editing, Writing – original draft, Formal analysis. **Shosei Kishida:** Writing – original draft, Resources. **Stefano Fedele:** Writing – review & editing, Writing – original draft, Funding acquisition. **Ipsita Roy:** Writing – review & editing, Writing – original draft, Project administration, Funding acquisition, Formal analysis, Conceptualization. **Jonathan C. Knowles:** Writing – review & editing, Writing – original draft, Supervision, Conceptualization.

Declaration of competing interest

IR is a Director of PHAsT Limited (CSO), which develops biomedical-grade polyhydroxyalkanoates (PHAs) for a variety of applications, including healthcare. However, the material used in this work wasn't developed by PHAsT Limited and was produced in IR's laboratory.

Acknowledgements

We (JCK, IR, RAM, AMS, SF and HB) acknowledge the funding obtained from Engineering and Physical Science Research Council (EPSRC) [grant number EP/X022196/1, EP/X026108/1].HB and IR acknowledge funding from Kidney Research UK (KRUK) (Grant Number SU_006_20240626.

Appendix A. Supplementary data

Supplementary data to this article can be found online at https://doi.org/10.1016/j.mtadv.2026.101023.

Data availability

Data will be made available on request.

References

[1] F. Brako, J. Boateng, Transmucosal drug delivery: prospects, challenges, advances, and future directions, Expert Opin. Drug Deliv. 22 (4) (2025) 525–553, https://doi.org/10.1080/17425247.2025.2470224. PubMed PMID: 39976299.
[2] I. Bácskay, P. Arany, P. Fehér, L. Józsa, G. Vasvári, D. Nemes, et al., Bioavailability enhancement and formulation technologies of oral mucosal dosage forms: a review, Pharmaceutics 17 (2) (2025 Feb 1), https://doi.org/10.3390/pharmaceutics17020148.
[3] S. Bahraminejad, H. Almoazen, Sublingual and buccal delivery: a historical and scientific prescriptive, Pharmaceutics 17 (8) (2025 Aug 1), https://doi.org/10.3390/pharmaceutics17081073.
[4] M. Sattar, O.M. Sayed, M.E. Lane, Oral transmucosal drug delivery - current status and future prospects, Elsevier, 2014, pp. 498–506, https://doi.org/10.1016/j.ijpharm.2014.05.043. PubMed PMID: 24879936 Int. J. Pharm.
[5] M.E. Mauceri, M. Coppini, V. De Caro, G. Di Prima, R. Mauceri, V. Panzarella, et al., Mucoadhesive drug delivery systems for oral chronic inflammatory mucosal diseases. The future is already present. A systematic review, Oral Dis. (2025 Jan 1), https://doi.org/10.1111/odi.70042.
[6] M.Á. González-Moles, S. Warnakulasuriya, I. González-Ruiz, L. González-Ruiz, Á. Ayén, D. Lenouvel, et al., Worldwide prevalence of oral lichen planus: a systematic review and meta-analysis, Oral Dis. 27 (4) (2021 May 1) 813–828, https://doi.org/10.1111/odi.13323. PubMed PMID: 32144836.
[7] N. Sengupta, S.C. Sarode, G.S. Sarode, R. Anand, D. Gopalakrishnan, Inefficacy of treatment modalities of oral lichen planus: evidence-based results, Oral Oncol. Rep. (2024 Mar 1) 9, https://doi.org/10.1016/j.oor.2024.100165.
[8] M. Carbone, P.G. Arduino, M. Carrozzo, G. Caiazzo, R. Broccoletti, D. Conrotto, et al., Topical clobetasol in the treatment of atrophic-erosive oral lichen planus: a randomized controlled trial to compare two preparations with different concentrations, J. Oral Pathol. Med. 38 (2009) 227–233, https://doi.org/10.1111/j.1600-0714.2008.00688.x.
[9] E.L. Myers, A.N. Hollis, D.A. Culton, Effectiveness and tolerability of systemic therapies in oral lichen planus: a retrospective cohort study, J. Am. Acad. Dermatol. 15 (2024 Oct 4) 136–138, https://doi.org/10.3389/fmed.2022.997190.
[10] T. Chintha, B. P, R. A, K.T. M, R. S, Translational research in oral lichen planus: from laboratory discoveries to clinical applications, Cureus (2024 Oct 14), https://doi.org/10.7759/cureus.71462.
[11] R. Binnie, M.L. Dobson, A. Chrystal, K. Hijazi, Oral lichen planus and lichenoid lesions - challenges and pitfalls for the general dental practitioner, Br. Dent. J. 236 (4) (2024 Feb 23) 285–292, https://doi.org/10.1038/s41415-024-7063-y. PubMed PMID: 38388599.
[12] P. de FR. Remiro, M.H.T. Nagahara, R.A. Azoubel, M. Franz-Montan, M.A. d'Ávila, Â.M. Moraes, Polymeric biomaterials for topical drug delivery in the oral cavity:

advances on devices and manufacturing technologies, Pharmaceutics 15 (1) (2023 Jan 1), https://doi.org/10.3390/pharmaceutics15010012.
[13] N.V. Dubashynskaya, V.A. Petrova, Y.A. Skorik, Biopolymer drug delivery systems for oromucosal application: recent trends in pharmaceutical R&D, Int. J. Mol. Sci. 25 (10) (2024 May 1), https://doi.org/10.3390/ijms25105359. PubMed PMID: 38791397.
[14] D. Kida, T. Konopka, K. Jurczyszyn, B. Karolewicz, Technological aspects and evaluation methods for polymer matrices as dental drug carriers, Biomedicines 11 (5) (2023 May 1), https://doi.org/10.3390/biomedicines11051274.
[15] Y. Tian, M. Orlu, H.J. Woerdenbag, M. Scarpa, O. Kiefer, D. Kottke, et al., Oromucosal films: from patient centricity to production by printing techniques, Expert Opin. Drug Deliv. 16 (9) (2019 Sep 2) 981–993, https://doi.org/10.1080/17425247.2019.1652595. PubMed PMID: 31382842.
[16] S. Tabakoglu, D. Kołbuk, P. Sajkiewicz, Multifluid electrospinning for multi-drug delivery systems: pros and cons, challenges, and future directions, Biomater. Sci. 11 (1) (2022 Oct 19) 37–61, https://doi.org/10.1039/d2bm01513g. PubMed PMID: 36367316.
[17] C.H. Mi, X.Y. Qi, Y.W. Ding, J. Zhou, J.W. Dao, D.X. Wei, Recent advances of medical polyhydroxyalkanoates in musculoskeletal system, Biomaterials Translational 4 (4) (2023) 234–247, https://doi.org/10.12336/biomatertransl.2023.04.004. PubMed PMID: 38282701.
[18] R. Nigmatullin, C.S. Taylor, P. Basnett, B. Lukasiewicz, A. Paxinou, L.R. Lizarraga-Valderrama, et al., Medium chain length polyhydroxyalkanoates as potential matrix materials for peripheral nerve regeneration, Regen. Biomater. 10 (2023), https://doi.org/10.1093/rb/rbad063.
[19] S.M.D. Syed Mohamed, J. Tuffin, J. Watson, A. Mele, A. Fricker, D.A. Gregory, et al., Biosynthesis, characterisation and biocompatibility of a unique and elastomeric medium chain-length polyhydroxyalkanoates for kidney glomerular tissue engineering, Mater. Today Bio 33 (2025 Aug 1), https://doi.org/10.1016/j.mtbio.2025.101932.
[20] W. Zhou, S. Bergsma, D.I. Colpa, G.J.W. Euverink, J. Krooneman, Polyhydroxyalkanoates (PHAs) synthesis and degradation by microbes and applications towards a circular economy, J. Environ. Manag. 341 (2023 Sep 1), https://doi.org/10.1016/j.jenvman.2023.118033. PubMed PMID: 37156023.
[21] Neoh S. Zher, Chek M. Fey, H. Tiang Tan, J.A. Linares-Pastén, A. Nandakumar, T. Hakoshima, et al., Polyhydroxyalkanoate synthase (PhaC): the key enzyme for biopolyester synthesis, Curr Res Biotechnol 4 (2022 Jan 1) 87–101, https://doi.org/10.1016/j.crbiot.2022.01.002.
[22] D. Solarz, T. Witko, R. Karcz, I. Malagurski, M. Ponjavic, S. Levic, et al., Biological and physiochemical studies of electrospun polylactid/polyhydroxyoctanoate PLA/P(3HO) scaffolds for tissue engineering applications, RSC Adv. 13 (34) (2023 Aug 11) 24112–24128, https://doi.org/10.1039/d3ra03021k.
[23] R.A. Macartney, A.T.R. Fricker, G.U.N. Tajalla, A.M. Smith, S. Kishida, S. Fedele, et al., Optimisation of electrospinning parameters to successfully obtain high ratios of medium chain length polyhydroxyalkanoate in electrospun fibres with drug loading for wound healing applications, J. Mater. Sci. Mater. Med. 37 (1) (2026 Dec 1), https://doi.org/10.1007/s10856-026-07030-5. PubMed PMID: 41886135.
[24] Z. Bazargani, M. Khorram, K. Zomorodian, M. Ghahartars, N. Omidifar, Development and comparative analysis of clobetasol-loaded microneedle patches versus clobetasol propionate ointment in experimental induced-psoriasis model, Int. J. Pharm. 674 (2025 Apr 15), https://doi.org/10.1016/j.ijpharm.2025.125423. PubMed PMID: 40074158.
[25] A. Mushtaq, A. Baseer, S.S. Zaidi, M. Waseem Khan, S. Batool, E. Elahi, et al., Fluconazole-loaded thermosensitive system: in vitro release, pharmacokinetics and safety study, J. Drug Deliv. Sci. Technol. (2022 Jan 1) 67, https://doi.org/10.1016/j.jddst.2021.102972.
[26] O.T. Ogedengbe, O.M. Kolawole, Formulation and evaluation of fluconazole emulgels for potential treatment of vaginal candidiasis, Heliyon 10 (6) (2024 Mar 30) e28206, https://doi.org/10.1016/j.heliyon.2024.e28206.
[27] D. Semnani, M. Afrashi, F. Alihosseini, P. Dehghan, M. Maherolnaghsh, Investigating the performance of drug delivery system of fluconazole made of nano–micro fibers coated on cotton/polyester fabric, J. Mater. Sci. Mater. Med. 28 (11) (2017 Nov 1), https://doi.org/10.1007/s10856-017-5957-9. PubMed PMID: 28956211.
[28] R.A. Macartney, A.T.R. Fricker, A.M. Smith, S. Fedele, I. Roy, J.C. Knowles, A RP-HPLC-UV method for the dual detection of fluconazole and clobetasol propionate and application to a model dual drug delivery hydrogel, Anal. Methods (2025 Apr 24), https://doi.org/10.1039/d4ay02219j.
[29] R. Sharma, T. Garg, A.K. Goyal, G. Rath, Development, optimization and evaluation of polymeric electrospun nanofiber: a tool for local delivery of fluconazole for management of vaginal candidiasis, Artif. Cells, Nanomed. Biotechnol. 44 (2) (2016 Jan 1) 524–531, https://doi.org/10.3109/21691401.2014.966194. PubMed PMID: 25315503.
[30] M. Afrashi, M. Nasari, D. Semnani, P. Dehghan, M. Maheronnaghsh, Comparison of the antifungal activity of fluconazole-and ketoconazole-loaded PCL/PVP nanofibrous mat, Bull. Mater. Sci. 44 (166) (2021) 1–9, https://doi.org/10.1007/s12034-021-02456-9S.
[31] R. Jiffrin, S.I.A. Razak, M.I. Jamaludin, A.S.A. Hamzah, M.A. Mazian, M.A.T. Jaya, et al., Electrospun nanofiber composites for drug delivery: a review on current progresses, Polymers 14 (18) (2022 Sep 1), https://doi.org/10.3390/polym14183725.
[32] M.S. Jose, S. Sumathi, A review of electrospun polymeric fibers as potential drug delivery systems for tunable release kinetics, J. Sci. Adv. Mater. Devices 10 (3) (2025 Sep 1), https://doi.org/10.1016/j.jsamd.2025.100933.
[33] L. Li, R. Hao, J. Qin, J. Song, X. Chen, F. Rao, et al., Electrospun fibers control drug delivery for tissue regeneration and cancer therapy, Adv. Fiber Mater. 4 (6) (2022 Dec 1) 1375–1413, https://doi.org/10.1007/s42765-022-00198-9.
[34] K. Flügel, K. Schmidt, L. Mareczek, M. Gäbe, R. Hennig, M. Thommes, Impact of incorporated drugs on material properties of amorphous solid dispersions, Eur. J. Pharm. Biopharm. 159 (2021 Feb 1) 88–98, https://doi.org/10.1016/j.ejpb.2020.12.017. PubMed PMID: 33383170.
[35] P. Tipduangta, P. Belton, W.J. McAuley, S. Qi, The use of polymer blends to improve stability and performance of electrospun solid dispersions: the role of miscibility and phase separation, Int. J. Pharm. (2021 Jun 1) 602, https://doi.org/10.1016/j.ijpharm.2021.120637. PubMed PMID: 33901595.
[36] R.F. Gibson, Principles of Composite Material Mechanics, fourth ed., CRC Press, 2016 https://doi.org/10.1201/b19626.
[37] R.F. Landel, L.E. Nielsen, Mechanical Properties of Polymers and Composites, second ed., CRC Press, 1993 https://doi.org/10.1201/b16929.
[38] J. Chen, R. Ahmad, W. Li, M. Swain, Q. Li, Biomechanics of oral mucosa, Royal Society of London, J. R. Soc. Interface (2015), https://doi.org/10.1098/rsif.2015.0325. PubMed PMID: 26224566.
[39] P. Tonglairoum, T. Ngawhirunpat, T. Rojanarata, S. Panomsuk, R. Kaomongkolgit, P. Opanasopit, Fabrication of mucoadhesive chitosan coated polyvinylpyrrolidone/cyclodextrin/clotrimazole sandwich patches for oral candidiasis, Carbohydr. Polym. 132 (2015 Jul 6) 173–179, https://doi.org/10.1016/j.carbpol.2015.06.032. PubMed PMID: 26256338.
[40] R. Olmos-Juste, B. Alonso-Lerma, R. Pérez-Jiménez, N. Gabilondo, A. Eceiza, 3D printed alginate-cellulose nanofibers based patches for local curcumin administration, Carbohydr. Polym. 264 (2021 Jul 15), https://doi.org/10.1016/j.carbpol.2021.118026. PubMed PMID: 33910718.
[41] S. Khan, J.S. Boateng, J. Mitchell, V. Trivedi, Formulation, characterisation and stabilisation of buccal films for paediatric drug delivery of omeprazole, AAPS PharmSciTech 16 (4) (2015 Aug 25) 800–810, https://doi.org/10.1208/s12249-014-0268-7. PubMed PMID: 25559373.
[42] D.M. Miu, M.C. Eremia, M. Moscovici, Polyhydroxyalkanoates (PHAs) as biomaterials in tissue engineering: production, isolation, characterization, Materials (2022), https://doi.org/10.3390/ma15041410. MDPI.
[43] T.R. Shamala, M.S. Divyashree, R. Davis, K.S.L. Kumari, S.V.N. Vijayendra, B. Raj, Production and characterization of bacterial polyhydroxyalkanoate copolymers and evaluation of their blends by fourier transform infrared spectroscopy and scanning electron microscopy, Indian J. Microbiol. 49 (2009 Sep) 251–258, https://doi.org/10.1007/s12088-009-0031-z.
[44] P. Tanikkul, G.L. Sullivan, S. Sarp, N. Pisutpaisal, Biosynthesis of medium chain length polyhydroxyalkanoates (mcl-PHAs) from palm oil, Case Stud. Chem. Environ. Eng. 2 (2020 Sep 1), https://doi.org/10.1016/j.cscee.2020.100045.
[45] T. Rakkan, N. Chana, K. Sangkharak, The integration of textile wastewater treatment with polyhydroxyalkanoate production using newly isolated enterobacter strain TS3, Waste Biomass Valor. 13 (1) (2022 Jan 1) 571–582, https://doi.org/10.1007/s12649-021-01504-z.
[46] Z. Mohammadalizadeh, E. Bahremandi-Toloue, S. Karbasi, Synthetic-based blended electrospun scaffolds in tissue engineering applications, J. Mater. Sci. 57 (6) (2022 Feb 1) 4020–4079, https://doi.org/10.1007/s10853-021-06826-w.
[47] S. Alghanem, E. Dziurkowska, I. Ordyniec-Kwaśnica, M. Sznitowska, Intraoral medical devices for sustained drug delivery, Springer Science and Business Media Deutschland GmbH, Clin. Oral Invest. (2023) 7157–7169, https://doi.org/10.1007/s00784-023-05377-5. PubMed PMID: 37982874.
[48] S.J. Pimlott, A. Addy, C. Wales, Evaluation of a method to study the uptake of prednisolone sodium phosphate from different oral mucosal sites, Oral Surg. Oral Med. Oral Pathol. 60 (1) (1985) 35–37, https://doi.org/10.1016/0030-4220(85)90211-7.
[49] N. Akhtar, M. Brizuela, Oral Lichen planus [Internet]. Statpearls [Internet], 2026 [cited 2026 Apr 30], https://www.ncbi.nlm.nih.gov/books/NBK578201/.
[50] M.L. Laracuente, M.H. Yu, K.J. McHugh, Zero-order drug delivery: state of the art and future prospects, J. Contr. Release 327 (2020 Nov 10) 834–856, https://doi.org/10.1016/j.jconrel.2020.09.020. PubMed PMID: 32931897.
[51] M. Askarizadeh, N. Esfandiari, B. Honarvar, S.A. Sajadian, A. Azdarpour, Kinetic modeling to explain the release of medicine from drug delivery systems, ChemBioEng Rev. 10 (6) (2023 Dec 1) 1006–1049, https://doi.org/10.1002/cben.202300027.
[52] V. Rivero-Buceta, M.R. Aguilar, A.M. Hernández-Arriaga, F.G. Blanco, A. Rojas, M. Tortajada, et al., Anti-staphylococcal hydrogels based on bacterial cellulose and the antimicrobial biopolyester poly(3-hydroxy-acetylthioalkanoate-co-3-hydroxyalkanoate), Int. J. Biol. Macromol. 162 (2020 Nov 1) 1869–1879, https://doi.org/10.1016/j.ijbiomac.2020.07.289. PubMed PMID: 32777414.
[53] T. Tawonsawatruk, A. Panaksri, R. Hemstapat, P. Praenet, K. Rattanapinyopituk, S. Boonyagul, et al., Fabrication and biological properties of artificial tendon composite from medium chain length polyhydroxyalkanoate, Sci. Rep. 13 (1) (2023 Dec 1), https://doi.org/10.1038/s41598-023-48075-8. PubMed PMID: 38017019.
[54] Q.A. Majid, P. Pandey, M. Bellahcene, C.L. Grigsby, M.M. Stevens, V. Talman, et al., Melt electrowritten medium chain length polyhydroxyalkanoate cardiac patches for Post-MI cardiac regeneration, Mater. Today Bio (2025 Oct 1) 34, https://doi.org/10.1016/j.mtbio.2025.102256.
[55] N.V. Dubashynskaya, V.A. Petrova, M. Bialiauskaya, Z. Livanovich, K. Khainskaya, I.V. Gofman, et al., Chitosan-gelatin core patches with drug release-controlling hyaluronan or carrageenan barriers for oromucosal delivery of clobetasol propionate, Int. J. Biol. Macromol. 332 (2025 Dec 1), https://doi.org/10.1016/j.ijbiomac.2025.148447. PubMed PMID: 41125173.

[56] N.V. Dubashynskaya, V.A. Petrova, I.V. Kudryavtsev, A.S. Trulioff, A.A. Rubinstein, A.S. Golovkin, et al., Electrospinning of Chitosan–Halloysite nanotube biohybrid mats for clobetasol propionate delivery, Technologies 13 (3) (2025 Mar 1), https://doi.org/10.3390/technologies13030090.
[57] E. Mazzinelli, M. Messina, I. Favuzzi, F. Vincenzoni, A. Giannoccolo, I. Cacciotti, et al., Poly(lactic acid) fibers for sustained drug delivery: insights into release profiles and cellular interactions, Materials 18 (11) (2025 Jun 1), https://doi.org/10.3390/ma18112532.
[58] T. Kibe, M. Kishida, M. Kamino, M. Iijima, L. Chen, M. Habu, et al., Immortalization and characterization of normal oral epithelial cells without using HPV and SV40 genes, Oral Sci Int 8 (1) (2011 May) 20–28, https://doi.org/10.1016/S1348-8643(11)00009-7.
[59] R. Yang, X. Hu, X. Xie, H. Chen, H. Fang, L. Zhu, et al., Propionic acid targets the TLR4/NF-κB signaling pathway and inhibits LPS-induced intestinal barrier dysfunction: in vitro and in vivo studies, Front. Pharmacol. 11 (2020 Sep 18), https://doi.org/10.3389/fphar.2020.573475.
[60] L. Wang, D. Song, C. Wei, C. Chen, Y. Yang, X. Deng, et al., Telocytes inhibited inflammatory factor expression and enhanced cell migration in LPS-induced skin wound healing models in vitro and in vivo, J. Transl. Med. 18 (1) (2020 Feb 6), https://doi.org/10.1186/s12967-020-02217-y. PubMed PMID: 32028987.
[61] Y. Deldar, Y. Pilehvar-Soltanahmadi, M. Dadashpour, S. Montazer Saheb, M. Rahmati-Yamchi, N. Zarghami, An in vitro examination of the antioxidant, cytoprotective and anti-inflammatory properties of chrysin-loaded nanofibrous mats for potential wound healing applications, Artif. Cells, Nanomed. Biotechnol. 46 (4) (2018 May 19) 706–716, https://doi.org/10.1080/21691401.2017.1337022. PubMed PMID: 28595461.
[62] P. Heydari, A. Zargar Kharazi, L. Shariati, Enhanced wound regeneration by PGS/PLA fiber dressing containing platelet-rich plasma: an in vitro study, Sci. Rep. 14 (1) (2024 Dec 1), https://doi.org/10.1038/s41598-024-62855-w. PubMed PMID: 38797743.
[63] K. Jantakee, J.N. Ferreira, P. Limlawan, Current in vitro models of oral Lichen Planus for investigating pathogenesis and facilitating drug discovery: a narrative review, J. Oral Pathol. Med. 55 (4) (2026 Apr 1) 419–428, https://doi.org/10.1111/jop.70101. PubMed PMID: 41388236.
[64] T. Shiohara, N. Moriya, T. Mochizuki, M. Nagashima, Lichenoid tissue reaction (LTR) induced by local transfer of Ia-Reactive T-Cell clones. II. LTR by epidermal invasion of cytotoxic lymphokine-producing autoreactive T cells, J. Invest. Dermatol. 89 (1) (1987) 814.
[65] D.W. Thomas, J.B. Matthews, S.S. Prime, Mucosal cell-mediated immunological changes associated with experimental graft-versus-host disease, J. Oral Pathol. Med. 25 (4) (1996) 145–150, https://doi.org/10.1111/j.1600-0714.1996.tb00211.x.
[66] A. Dunsche, M.P. Frank, J. Lüttges, Y. Açil, J. Brasch, E. Christophers, et al., Lichenoid reactions of Murine mucosa associated with amalgam, Br. J. Dermatol. 148 (2003) 741–748.
[67] M. Li, Y. Yu, Innate immune receptor clustering and its role in immune regulation, J. Cell Sci. 134 (4) (2021 Feb 1), https://doi.org/10.1242/jcs.249318. PubMed PMID: 33597156.
[68] C. Peetla, A. Stine, V. Labhasetwar, Biophysical interactions with model lipid membranes: applications in drug discovery and drug delivery, Mol. Pharm. 6 (5) (2009 Oct 5) 1264–1276, https://doi.org/10.1021/mp9000662. PubMed PMID: 19432455.
[69] S.W. Wong, M.J. Kwon, A.M.K. Choi, H.P. Kim, K. Nakahira, D.H. Hwang, Fatty acids modulate toll-like receptor 4 activation through regulation of receptor dimerization and recruitment into lipid rafts in a reactive oxygen species-dependent manner, J. Biol. Chem. 284 (40) (2009 Oct 2) 27384–27392, https://doi.org/10.1074/jbc.M109.044065. PubMed PMID: 19648648.
[70] C. Hellwing, A. Schoeniger, C. Roessler, A. Leimert, J. Schumann, Lipid raft localization of TLR2 and its co-receptors is independent of membrane lipid composition, PeerJ (2018), https://doi.org/10.7717/peerj.4212, 2018(1).
[71] Z. Wan, Y. Yu, Q. Cheng, W. Tang, W. Tan, M. Liu, Rational design of hydrogel polymer nanoparticles based on a receptor recognition mechanism of endotoxin and its application in endotoxin removal, ACS Appl. Polym. Mater. 6 (23) (2024 Dec 13) 14490–14504, https://doi.org/10.1021/acsapm.4c02545.
[72] M. Alipour, E. Habibivand, S. Sekhavati, Z. Aghazadeh, M. Ranjkesh, S. Ramezani, et al., Evaluation of therapeutic effects of nanofibrous mat containing mycophenolate mofetil on oral lichen planus: in vitro and clinical trial study, Biomater Investig Dent 10 (1) (2023), https://doi.org/10.1080/26415275.2023.2283177.
[73] Z. Said, C. Murdoch, J. Hansen, L. Siim Madsen, H.E. Colley, Corticosteroid delivery using oral mucosa equivalents for the treatment of inflammatory mucosal diseases, Eur. J. Oral Sci. 129 (2) (2021 Apr 1), https://doi.org/10.1111/eos.12761. PubMed PMID: 33645844.
[74] M. Bitzer, G. Von Gersdorff, D. Liang, A. Dominguez-Rosales, A.A. Beg, M. Rojkind, et al., A mechanism of suppression of TGF-/SMAD signaling by NF-B/RelA, Genes Dev. 14 (2000) 187–197 [Internet], www.genesdev.org.
[75] X. Yan, Z. Liu, Y. Chen, Regulation of TGF-β signaling by Smad7, Acta Biochim. Biophys. Sin. 41 (4) (2009 Apr) 263–272, https://doi.org/10.1093/abbs/gmp018. PubMed PMID: 19352540.
[76] K. Mitchell, J.P. Shah, L.V. Tsytsikova, A.M. Campbell, K. Affram, A.J. Symes, LPS antagonism of TGF-β signaling results in prolonged survival and activation of rat primary microglia, J. Neurochem. 129 (1) (2014) 155–168, https://doi.org/10.1111/jnc.12612. PubMed PMID: 24251648.
[77] R.M. Liu, L.P. Desai, Reciprocal regulation of TGF-β and reactive oxygen species: a perverse cycle for fibrosis, Redox Biol. 6 (2015 Dec 1) 565–577, https://doi.org/10.1016/j.redox.2015.09.009. PubMed PMID: 26496488.
[78] J. Liu, X. Han, T. Zhang, K. Tian, Z. Li, F. Luo, Reactive oxygen species (ROS) scavenging biomaterials for anti-inflammatory diseases: from mechanism to therapy, J. Hematol. Oncol. 16 (1) (2023 Dec 1), https://doi.org/10.1186/s13045-023-01512-7. PubMed PMID: 38037103.
[79] M.J. Page, D.B. Kell, E. Pretorius, The role of lipopolysaccharide-induced cell signalling in chronic inflammation, Chronic Stress 6 (2022 Feb 1), https://doi.org/10.1177/24705470221076390.